

Azepanone-Based Inhibitors of Human and Rat Cathepsin K

Robert W. Marquis,^{*,†} Yu Ru,[†] Steven M. LoCastro,[†] Jin Zeng,[†] Dennis S. Yamashita,[†] Hye-Ja Oh,[†] Karl F. Erhard,[†] Larry D. Davis,[†] Thaddeus A. Tomaszek,[‡] David Tew,[‡] Kevin Salyers,[§] Joel Proksch,[§] Keith Ward,[§] Brian Smith,[§] Mark Levy,[§] Maxwell D. Cummings,^{||,1} R. Curtis Haltiwanger,^{||} Gudrun Trescher,^{||} Bing Wang,^{||} Mark E. Hemling,^{||} Chad J. Quinn,^{||} H-Y. Cheng,^{||} Fan Lin,^{||} Ward W. Smith,[⊥] Cheryl A. Janson,[⊥] Baoguang Zhao,[⊥] Michael S. McQueney,[#] Karla D'Alessio,[#] Chao-Pin Lee,[⊙] Antonia Marzulli,[§] Robert A. Dodds,^{^,2} Simon Blake,[^] Shing-Mei Hwang,[^] Ian E. James,[^] Catherine J. Gress,[^] Brian R. Bradley,[^] Michael W. Lark,[^] Maxine Gowen,[^] and Daniel F. Veber^{*,†}

Departments of Medicinal Chemistry, Mechanistic Enzymology, Drug Metabolism and Pharmacokinetics, Physical and Structural Chemistry, Structural Biology, Protein Biochemistry, Life-Cycle Management and Drug Delivery Systems, and Bone and Cartilage Biology, GlaxoSmithKline, 709 Swedeland Road, King of Prussia, Pennsylvania 19406

Received November 10, 2000

The synthesis, in vitro activities, and pharmacokinetics of a series of azepanone-based inhibitors of the cysteine protease cathepsin K (EC 3.4.22.38) are described. These compounds show improved configurational stability of the C-4 diastereomeric center relative to the previously published five- and six-membered ring ketone-based inhibitor series. Studies in this series have led to the identification of **20**, a potent, selective inhibitor of human cathepsin K ($K_i = 0.16$ nM) as well as **24**, a potent inhibitor of both human ($K_i = 0.0048$ nM) and rat ($K_{i,app} = 4.8$ nM) cathepsin K. Small-molecule X-ray crystallographic analysis of **20** established the C-4 *S* stereochemistry as being critical for potent inhibition and that unbound **20** adopted the expected equatorial conformation for the C-4 substituent. Molecular modeling studies predicted the higher energy axial orientation at C-4 of **20** when bound within the active site of cathepsin K, a feature subsequently confirmed by X-ray crystallography. Pharmacokinetic studies in the rat show **20** to be 42% orally bioavailable. Comparison of the transport of the cyclic and acyclic analogues through CaCo-2 cells suggests that oral bioavailability of the acyclic derivatives is limited by a P-glycoprotein-mediated efflux mechanism. It is concluded that the introduction of a conformational constraint has served the dual purpose of increasing inhibitor potency by locking in a bioactive conformation as well as locking out available conformations which may serve as substrates for enzyme systems that limit oral bioavailability.

Introduction

Cathepsin K (EC 3.4.22.38), a 24-kDa cysteine protease of the papain superfamily, has been shown to be selectively expressed within osteoclasts as a proenzyme.¹ Upon activation, mature cathepsin K is secreted from the osteoclast into the acidic resorption lacuna where it plays a critical role in the degradation of the protein matrix of bone. Several studies have reinforced the role of cathepsin K in bone resorption and highlighted the attractiveness of this cysteine protease as a target for inhibition in diseases characterized by elevated levels of bone turnover such as osteoporosis.^{2–4}

Recently the evolution of a variety of templates targeting the inhibition of cysteine proteases has begun

to expand.⁵ This expansion is based upon several studies which have shown that members of this class of protease are expressed selectively and that they play a critical role in the pathology of disease. The design and activity of a new class of reversible, 1,3-bis(acylamino)-2-propanone inhibitors of cathepsin K, exemplified by **1**, have been reported (Figure 1).⁶ Despite potent inhibition of cathepsin K, the low oral bioavailability, short duration of action, and low potency in cell-based assays of bone resorption limited the utility of this class of compounds. Initial attempts to address these issues focused on the incorporation of peptidomimetic elements designed to reduce the peptide nature of **1**. This has led to the discovery of compounds **2** and **3** which are potent inhibitors of human cathepsin K displaying potent inhibition in cell-based assays of bone resorption.⁷ However, because both **2** and **3** displayed poor oral bioavailability in the rat, their utility was limited to subcutaneous and intraperitoneal routes of administration. A particularly successful modification of **1**, involving the introduction of a conformational constraint, has led to the previously reported 3-amido-pyrrolidin-4-one **4** and the 4-amido-piperidin-3-one **5**, both of which are potent, reversible inhibitors of cathepsin K.^{8,9} Several analogues within these cyclic 1,3-diaminoketone series displayed promising preliminary pharmacokinetics as

* Corresponding authors: Dept. of Medicinal Chemistry, Glaxo-SmithKline, 709 Swedeland Rd., P.O. Box 1539, UW 24-1055, King of Prussia, PA 19406. Phone: 610-270-6570/6561. Fax: 610-270-4451. E-mail: robert_w_marquis@sbphrd.com or daniel_f_veber@sbphrd.com.

[†] Department of Medicinal Chemistry.

[‡] Department of Mechanistic Enzymology.

[§] Department of Drug Metabolism and Pharmacokinetics.

^{||} Department of Physical and Structural Chemistry.

[⊥] Department of Structural Biology.

[#] Department of Protein Biochemistry.

[⊙] Department of Life-Cycle Management and Drug Delivery Systems.

[^] Department of Bone and Cartilage Biology.

¹ Current address: 3-Dimensional Pharmaceuticals Inc., 665 Stockton Dr., Eaglevie Corporate Center, Exton, PA 19341.

² Current address: Osiris Therapeutics Inc., 2001 Aliceanne St., Baltimore, MD 21207.

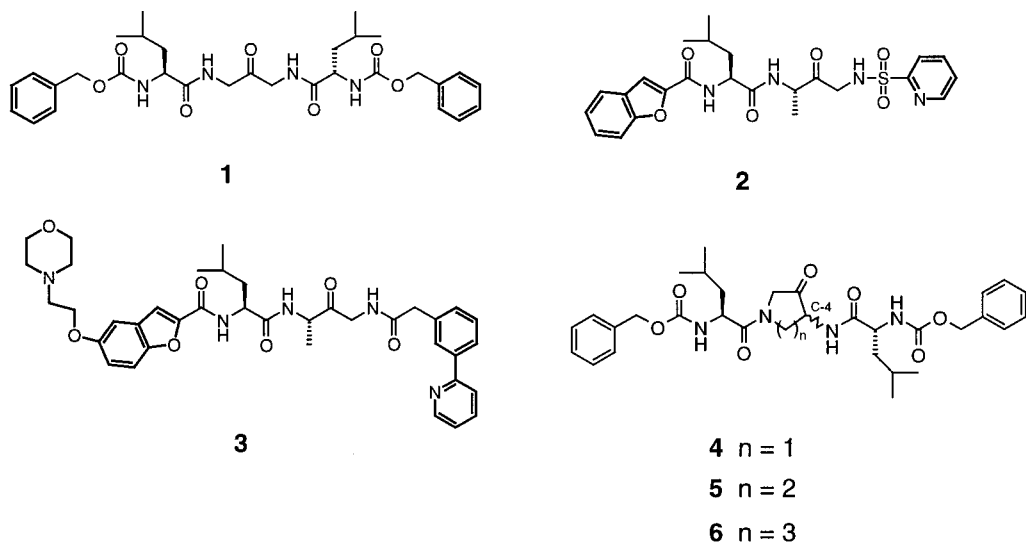


Figure 1. Templates leading to azepanone inhibitors.

well as adequate potency versus rat cathepsin K.¹⁰ Due to rapid epimerization of the C-4 chiral center contained within these inhibitors, they were unsuitable for more detailed analyses of their pharmacokinetics in either rodents or primates. The rapid rate of epimerization of the C-4 diastereomeric center associated with these analogues represents a significant pharmacokinetic issue since it is difficult to determine whether the more potent of the two diastereomers has been absorbed and is actually present in the blood. The timelines of the analytical methods employed for the pharmacokinetic analysis of compounds is normally long relative to the epimerization rates of these inhibitors. On the other hand, inhibitor epimerization is of a time scale such that equilibration may not occur in blood prior to excretion. As such, the chiral instability present in the five- and six-membered ring cyclic diaminoketones would lead to racemization prior to serum analysis. The reality of this situation is fully recognized by the stereoselective oral bioavailability of the chirally stable azepanones described in this paper.

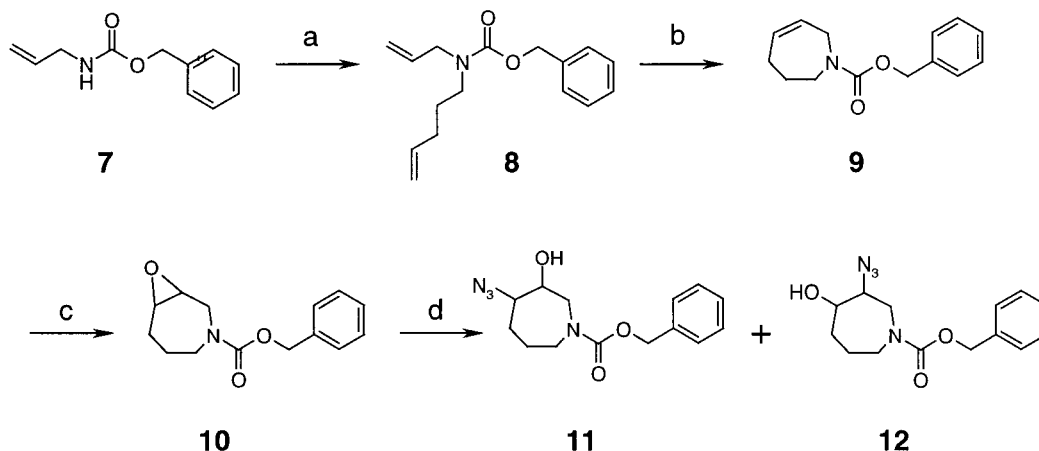
The combination of potent enzyme inhibition and promising, but inconclusive, pharmacokinetics of the five- and six-membered ring diaminoketones prompted the investigation of several strategies designed to eliminate the epimerization of the labile C-4 chiral center of these analogues. Initial attempts to address this issue included blocking the offending epimerization by incorporation of a methyl group at C-4 or by elimination of the ketone moiety. Although both of these strategies produced compounds capable of inhibiting cathepsin K, their potencies were substantially reduced relative to the unsubstituted or ketone analogues.¹¹ An ultimately successful approach to this epimerization issue was based on data which had shown that the rate of ketone enolization in the cyclic 1,3-diaminoketone series became slower as the heterocyclic ring was expanded from five to six members. Additionally, epimerization rates in the acyclic 1,3-diaminoketone series (see structure **2**, Figure 1) had also been shown to be negligible. These data suggested that further ring expansion could slow the rate of ketone enolization to a degree sufficient to address the pharmacokinetic issues described above.

In this paper we describe a series of configurationally stable, azepanone-based inhibitors of human cathepsin K. Ring expansion of the five- and six-membered ring cyclic 1,3-diaminoketone templates to a seven-membered ring azepanone such as **6** (Figure 1) has proven to be highly effective in improving the C-4 chiral stability of these inhibitors. This modification has simultaneously provided compounds with improved oral bioavailability in rats. Additionally, incorporation of functional groups derived from structure-activity studies (SARs) in the acyclic 1,3-diaminoketone series into this azepanone template has led to the identification of **20**, a potent, reversible inhibitor of human cathepsin K which displays good oral bioavailability in the rat, as well as inhibitor **24**, a potent inhibitor of both human and rat cathepsin K.

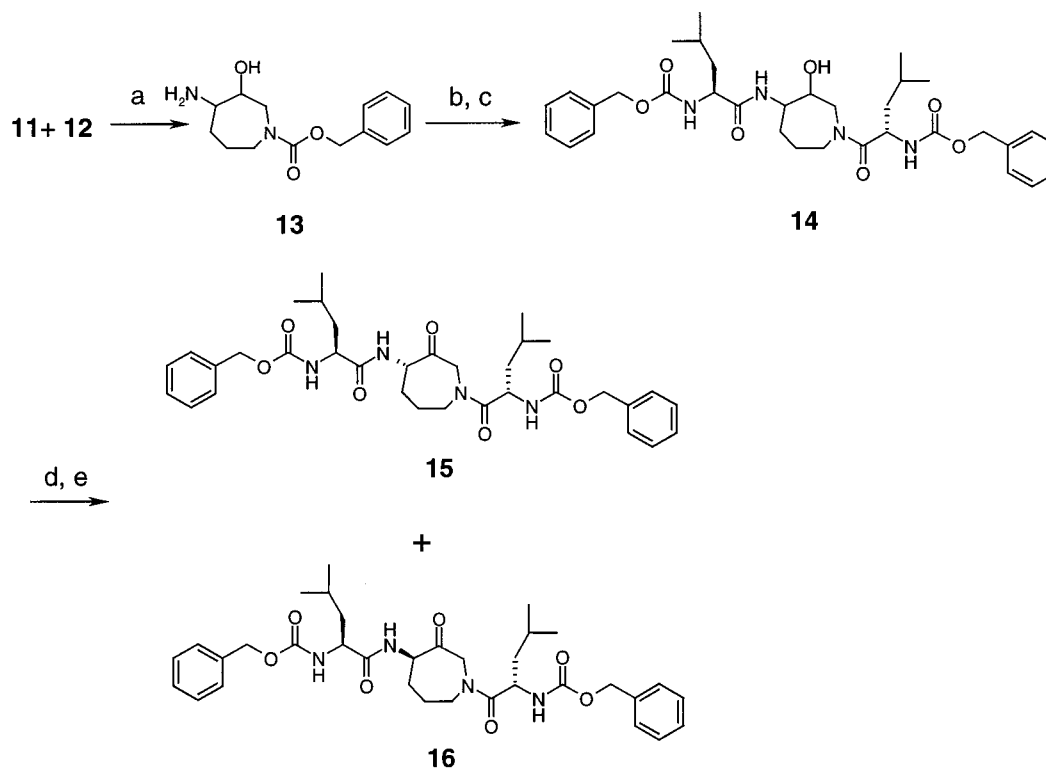
Synthesis Chemistry

The syntheses of the azepanone and acyclic diaminoketone inhibitors described in this paper are detailed in Schemes 1–7. As shown in Scheme 1, N-alkylation of benzyl *N*-allylcarbamate (**7**)¹² with 5-bromo-1-pentene in the presence of sodium hydride provided the olefin metathesis substrate **8**. Treatment of diene **8** with catalytic bis(tricyclohexylphosphine)benzylidineruthenium(IV) dichloride according to the procedure developed by Grubbs and co-workers¹³ cleanly effected the ring-closing olefin metathesis to provide azepine **9**. Epoxidation of **9** with *m*-CPBA provided oxirane **10** which was treated with sodium azide under standard conditions to cleanly afford azido alcohols **11** and **12** in a ratio of 9:1 (as determined by HPLC analysis) favoring the desired regioisomer **11**. The regioselectivity of this epoxide opening is likely the result of the preferred chair conformation of **10** which places the bulky carbonylbenzyloxy nitrogen protecting group in a pseudo-axial orientation. This conformation effectively blocks the C-3 carbon leading to the preferred trans-diaxial nucleophilic opening of the epoxide at C-4.¹⁴ The undesired azido alcohol **12** was carried through the synthesis sequence and was removed at a later stage.

Elaboration of the azepanone core to **15** and **16** is outlined in Scheme 2. The mixture of azides **11** and **12** was reduced with 1,3-propanedithiol in methanol and

Scheme 1. Synthesis of 4-Azido-3-hydroxyazepanes **11** and **12**^a

^a Reagents and conditions: (a) 5-bromo-1-pentene, NaH, DMF; (b) bis(tricyclohexylphosphine)benzylidineruthenium(IV) dichloride, CH₂Cl₂, reflux; (c) *m*-CPBA, CH₂Cl₂; (d) NaN₃, NH₄Cl, H₂O, CH₃OH, 70 °C.

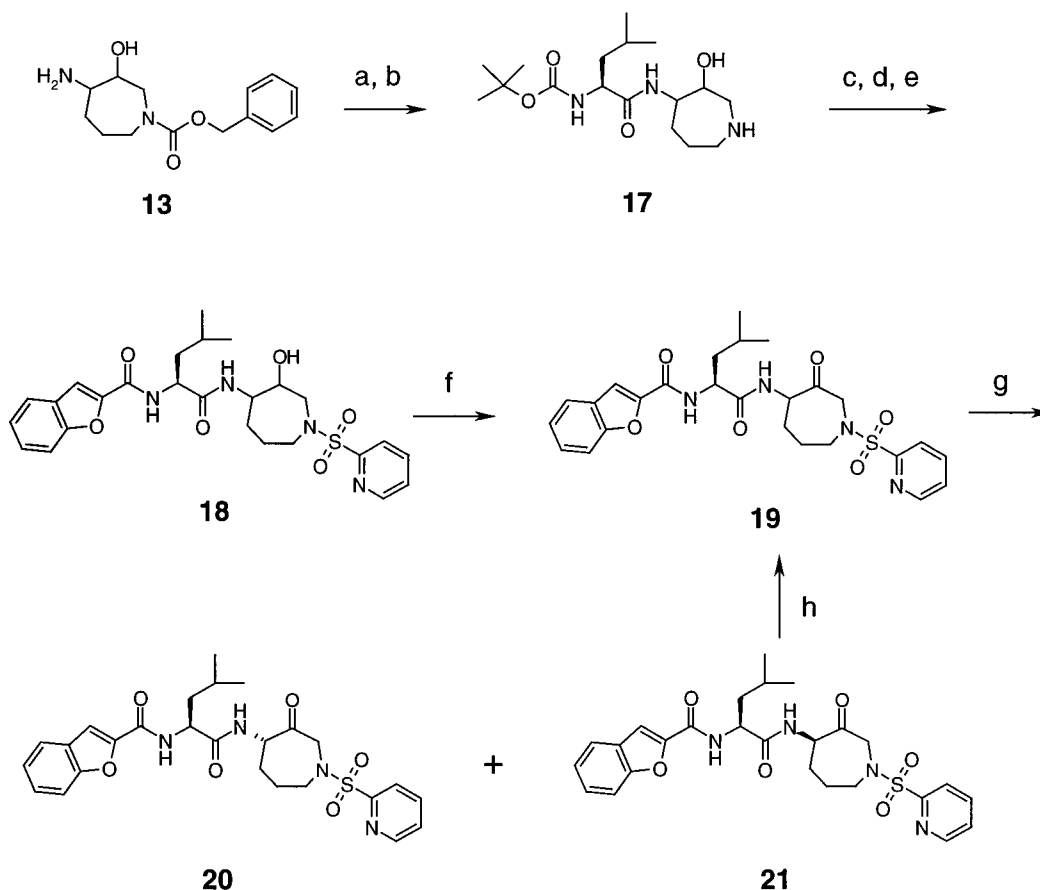
Scheme 2. Synthesis of Azepanones **15** and **16**^a

^a Reagents and conditions: (a) 1,3-propanedithiol, TEA, CH₃OH; (b) 10% Pd/C, H₂, CH₃OH; (c) Cbz-leucine, EDC, HOBT, CH₂Cl₂; (d) Dess–Martin periodinane, CH₂Cl₂; (e) HPLC separation.

triethylamine¹⁵ to provide the intermediate amino alcohol **13**. Hydrogenolysis of the benzyloxycarbonyl protecting group, followed by bis-acylation of the resulting 4-aminoazepan-3-ol (not shown) with 2 equiv of Cbz-leucine in the presence of EDC, provided the diastereomeric mixture of alcohols **14**. Oxidation of alcohols **14** followed by HPLC separation of the diastereomeric ketones provided azepanones **15** and **16**.

The syntheses of analogues **20** and **21** are detailed in Scheme 3. Acylation of amino alcohol **13** with *N*-Boc-leucine in the presence of EDC followed by hydrogenolysis of the carbonylbenzyloxy protecting group provided amine **17**. Treatment of **17** with freshly prepared 2-pyridinesulfonyl chloride in the presence of triethylamine followed by removal of the *tert*-butoxycarbonyl

protecting group and acylation of the resulting amine salt with benzofuran-2-carboxylic acid gave **18** as a mixture of two diastereomers. Application of the 2-pyridylsulfonamide moiety to the azepanone template had been derived from earlier work in the acyclic 1,3-diaminoketone series where this functionality was shown to be a potency-enhancing, Cbz-leucine peptidomimetic. Oxidation of the mixture **18** with pyridine sulfur trioxide complex¹⁶ gave the mixture of diastereomeric ketones **19** which were separated by HPLC to provide azepanones **20** and **21**. Diastereomer **21** could be recycled to **20** by epimerization with triethylamine in methanol and water followed by a second HPLC separation. The small-molecule X-ray crystal structure of **20** unequivocally established the stereochemistry of

Scheme 3. Synthesis of Azepanones **20** and **21**^a

^a Reagents and conditions: (a) *N*-Boc-leucine, EDC, HOBT, CH₂Cl₂; (b) 10% Pd/C, H₂, CH₃OH; (c) 2-pyridylsulfonyl chloride, TEA, CH₂Cl₂; (d) HCl, EtOAc, CH₃OH; (e) benzofuran-2-carboxylic acid, EDC; (f) SO₃-pyridine complex, TEA, DMSO; (g) HPLC separation; (h) TEA, CH₃OH, H₂O.

the C-4 chiral center as *S* (Figure 2). In this structure the azepanone ring is in a pseudo-boat conformation with the C-4 leucinamide group in an equatorial orientation.

As outlined in Scheme 4, the synthesis of **24** and **25** began with acylation of amine **17** with 2-(3-pyridin-2-phenyl)acetic acid¹⁷ in the presence of EDC. Removal of the *tert*-butoxycarbonyl protecting group followed by coupling of the resulting amine with 5-[2-(4-morpholinyl)ethoxy]-2-benzofuran-2-carboxylic acid provided **22** as a mixture of two diastereomers. Oxidation of the mixture **22** gave azepanones **23** as a 1:1 mixture of diastereomers which were separated by HPLC to provide **24** and **25**. Triethylamine-induced epimerization of **25** to the diastereomeric mixture of ketones **23** followed by a second HPLC separation allowed for a recycling of this less desired diastereomer.

The syntheses of acyclic inhibitors **2**, **28**, and **36** are outlined in Schemes 5–7. As shown in Scheme 5, acylation of the commercially available 1,3-diamino-2-hydroxypropane (**26**) with *N*-Boc-L-leucine in the presence of EDC followed by sulfonation with 2-pyridinesulfonyl chloride provided the alcohol intermediate **27**. Removal of the *N*-Boc protecting group and acylation of the resulting amine salt with benzofuran-2-carboxylic acid and oxidation provided ketone inhibitor **28**.

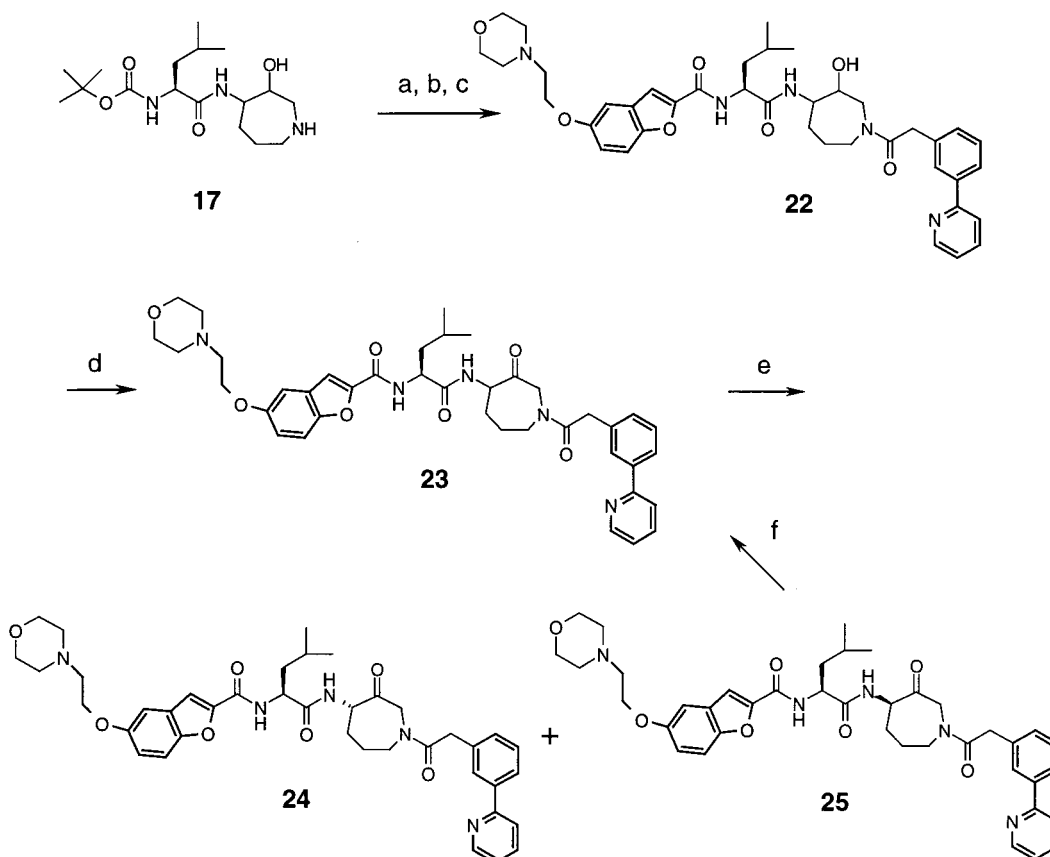
Scheme 6 details the synthesis of inhibitor **2**. Sulfonation of the known amino alcohol **29**¹⁸ with 2-py-

ridinesulfonyl chloride gave intermediate **30**. Removal of the *N*-Boc protecting group followed by acylation with *N*-Boc-L-leucine, deprotection, and acylation with benzofuran-2-carboxylic acid gave intermediate **32** which was oxidized with the Dess–Martin periodinane to provide ketone **2**.

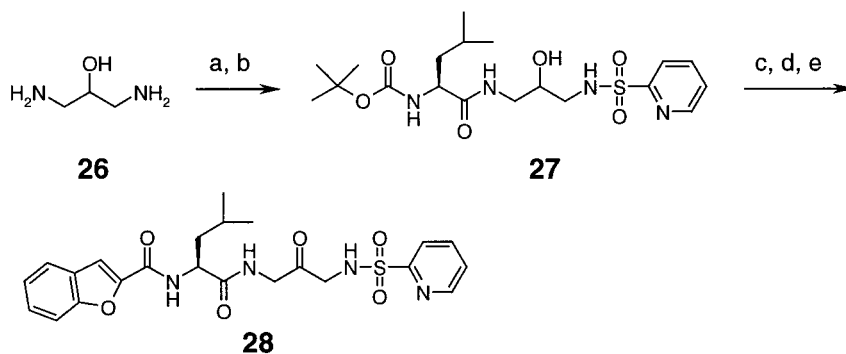
As shown in Scheme 7, treatment of the known epoxide **33**¹⁹ with *N*-methylamine followed by sulfonation with 2-pyridinesulfonyl chloride provided alcohol intermediate **34**. Removal of the *N*-Boc protecting group and acylation of the subsequent amine salt with *N*-Cbz-L-leucine gave alcohol **35**. Deprotection of **35** followed by acylation with benzofuran-2-carboxylic acid and oxidation provided ketone **36**.

Results and Discussion

Potencies and Selectivities. Studies of cyclic five- and six-membered ring ketone-derived cathepsin K inhibitors had highlighted the possibility of improved pharmacokinetics but had also shown that these ring systems were configurationally unstable at the C-4 diastereomeric center. As shown in Table 1, ring expansion to the azepanone **6** improved the stability of the C-4 chiral center to the point that separation of the individual diastereomers **15** and **16** was now possible. Azepanone **15** was shown to be a 2.0 nM inhibitor of cathepsin K, while diastereomer **16** was at least 7-fold less potent with a $K_{i,app} = 15$ nM. Inhibitor **15** was selective for cathepsin K versus cathepsins L ($K_{i,app} =$

Scheme 4. Synthesis of Inhibitors **24** and **25**^a

^a Reagents and conditions: (a) 2-(3-pyridin-2-ylphenyl)acetic acid, EDC, HOBT; (b) HCl, EtOAc, CH₃OH; (c) 5-[2-(4-morpholinyl)ethoxy]-2-benzofuran-2-carboxylic acid, EDC, HOBT; (d) SO₃-pyridine complex, TEA, DMSO; (e) HPLC separation; (f) TEA, CH₃OH, H₂O.

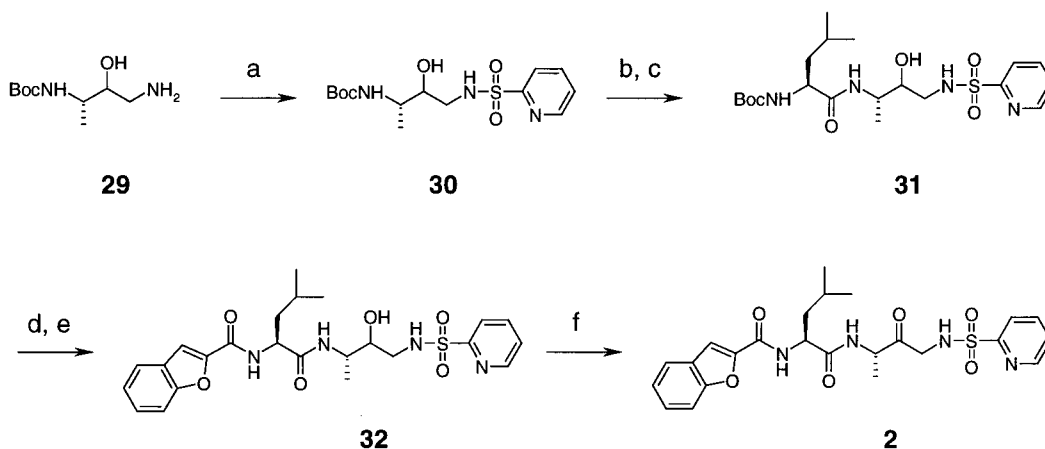
Scheme 5. Synthesis of Acyclic Inhibitor **28**^a

^a Reagents and conditions: (a) *N*-Boc-L-leucine, EDC, HOBT; (b) 2-pyridylsulfonyl chloride, NMM, CH₂Cl₂; (c) TFA; (d) benzofuran-2-carboxylic acid, HBTU, DMF; (e) Dess-Martin periodinane, CH₂Cl₂.

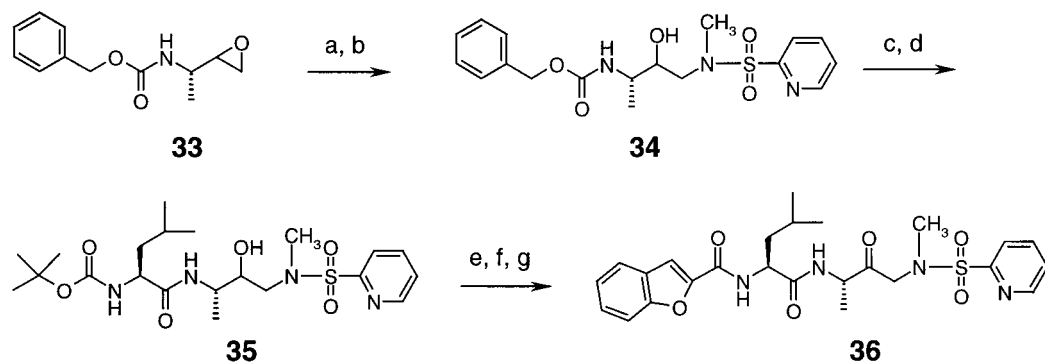
47 nM; cathepsins K/L = 23) and S ($K_{i,app} = 26$ nM; cathepsins K/S = 13). Azepanone **15** is 11-fold more potent than its acyclic counterpart **1** (cathepsin K $K_{i,app} = 22$ nM) highlighting the utility of a conformational constraint in locking in a bioactive conformation of this inhibitor.²⁰ Having established both the viability of the ring expansion concept for the potent inhibition of cathepsin K as well as the improved chiral stability of the C-4 diastereomeric center, this class of seven-membered ketones became the focus of a medicinal chemistry effort to optimize selectivity and oral bioavailability. Functional groups which had displayed potent inhibition of human and rat cathepsin K and had led to effective inhibition of native cathepsin K in cell- and tissue-based in vitro assays systems in the acyclic

1,3-diaminopropanone series were applied to this azepanone template.

As shown in Table 1, the incorporation of the 2-pyridinesulfonamide group, which had been shown in the acyclic 1,3-diaminopropanone series to be an effective potency-enhancing replacement for the Cbz-leucine moiety, combined with replacement of the carbonylbenzyloxy group with the benzofuran-2-carboxamide, provided **20** which is a potent inhibitor of human cathepsin K with a $K_i = 0.16$ nM. Analogue **20** is 13-fold selective for cathepsin K versus cathepsin L, 25-fold selective versus cathepsin S, and greater than 3000-fold selective versus cathepsin B. The C-4 *R* diastereomer **21** was approximately 1/6000th as active as **20** with a $K_{i,app} = 980$ nM, highlighting the critical nature of this center

Scheme 6. Synthesis of Inhibitor **2**^a

^a Reagents and conditions: (a) 2-pyridinesulfonyl chloride, NMM, DMF; (b) 4 M HCl/dioxane, CH₂Cl₂; (c) *N*-Boc-L-leucine, NMM, HBTU; (d) 4 M HCl/dioxane, CH₃OH; (e) benzofuran-2-carboxylic acid, HBTU, NMM; (f) Dess–Martin periodinane, CH₂Cl₂.

Scheme 7. Synthesis of Inhibitor **36**^a

^a Reagents and conditions: (a) *N*-methylamine, 2-propanol; (b) 2-pyridinesulfonyl chloride, NaHCO₃, CH₂Cl₂; (c) 10% Pd/C, H₂, EtOH, 10% HCl; (d) *N*-Boc-leucine, DIPEA, EDC, HOBt; (e) 4 M HCl/dioxane, CH₃OH; (f) benzofuran-2-carboxylic acid, DIPEA, HOBt, EDC; (g) Dess–Martin periodinane.

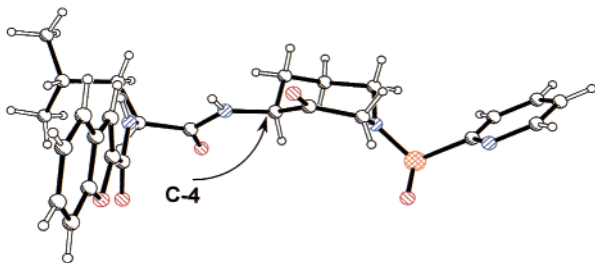


Figure 2. ORTEP representation of the small-molecule X-ray crystal structure of azepanone **20**. The C-4 chiral center is of the *S* configuration with the leucinamide group in an equatorial orientation off of the azepanone ring.

for potent inhibition of cathepsin K. (We are unable to exclude the possibility that even this low level of activity may be the result of contamination (<0.01%) by **20**.) The mixture of diastereomeric alcohols **18** was not active when tested up to a concentration of 1 μ M. The incorporation of a conformational constraint has increased the inhibitor potency of **20** at least 10-fold relative to acyclic analogues **28**, **2**, and **36** which are 1.6, 7.5, and 670 nM inhibitors of cathepsin K, respectively. Compound **20** has been characterized as a competitive, reversible inhibitor of cathepsin K. As shown in Figure 3 the Lineweaver–Burk plot of **20** displays a $1/v$ axis intercept which is constant with increasing inhibitor concentration, indicative of competitive inhibition. There was no time-dependent inhibi-

Table 1. Inhibitory Potencies versus Human Cathepsins K, L, S, B and Rat Cathepsin K and in Vitro Cell-Based Assays

compd	human ^b <i>K_i</i> (nM)				rat ^c <i>K_i</i> (nM)	IC ₅₀ (nM)	
	Cat K	Cat L	Cat S	Cat B		osteoclast resorption assay	in situ cytochem assay
1	22	340	890	1,300			
2	7.5		20	59			
4	2.3	39		>1000			
5	2.6	16		440			
6	30						
15	2.0	47	26				
16	15	290	97				
18 ^a	>1000						
20	0.16	2.2	4.0	500	60	70	
21	980						
22 ^a	54						
24	0.0048	0.49	14	100	4.8	30	
25	4.7						
28	1.6						
36	670						

^a Inhibitory potencies for alcohols **18** and **22** are reported as mixtures of diastereomers. ^b Inhibitory potencies versus cathepsins K, B, L and S were determined as describe in ref 6b. ^c Assay versus rat cathepsin K was performed as described in ref 25.

tion observed over a 30-min period. The reversible nature of inhibition of **20** was established by mass spectral analysis which showed that upon incubation of **20** with cathepsin K for 2 h there had been no irreversible modification of the protein by the inhibitor. Incubation of **20** with excess cysteine in D₂O/DMSO followed by ¹H NMR analysis showed **20** to be stable to

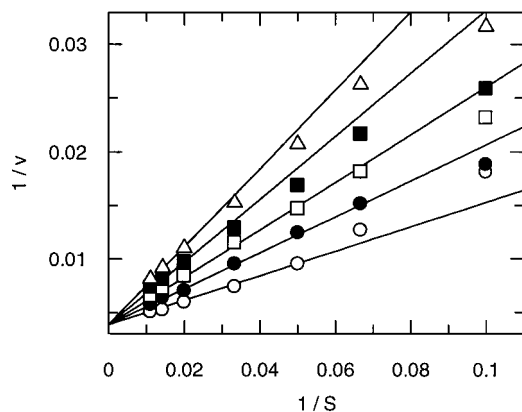


Figure 3. Lineweaver–Burk plot of **20** at increasing inhibitor concentrations of 0 nM (○), 100 nM (●), 200 nM (□), 350 nM (■), 500 nM (△).

Table 2. First-Order Rate Constants of Epimerization at pH 11 and 12.5

compd	k (s^{-1})	
	pH 11	pH 12.5
20 to 21	6.2×10^{-5}	1.7×10^{-3}
21 to 20	6.0×10^{-5}	2.3×10^{-3}
24 to 25	1.2×10^{-5}	2.2×10^{-4}
25 to 24	1.0×10^{-5}	2.9×10^{-4}

epimerization. Within the level of detection at 500 MHz, this experiment also showed no hemithioacetal formation highlighting the unreactive nature of the azepanone carbonyl moiety. Azepanone **20** is a potent inhibitor of native cathepsin K in an in vitro, cell-based assay of bone resorption²¹ ($IC_{50} = 70$ nM) as well as a potent inhibitor in an in situ cytochemical assay ($IC_{50} = 80$ nM) which measures cathepsin activity in osteoclasts in sections of human tissue.²²

An HPLC method allowing for the baseline separation of 1:1 diastereomeric mixtures of azepanones was developed in order to more precisely elucidate the rate of epimerization of the C-4 chiral center of this class of compound. Under acidic to neutral pH conditions (pH 2–7 phosphate buffer) the C-4 centers of the diastereomeric pair **20** and **21** were each stable in aqueous buffer for days with no detectable change by HPLC analysis. At pH > 12 these compounds epimerized rapidly to reach a 1:1 ratio within a few hours. Similar behaviors were observed for azepanones **24** and **25** and for the acyclic derivative **2**. To further elucidate the mechanism of enolization, kinetic studies in pH 11 and 12.5 buffers, in which the epimerization could be monitored in a reasonable experimental time frame, were carried out on **20**, **21**, and their corresponding 2,2',4-trideuterated analogues **37** and **38**.²³ The first-order rate constants of epimerization are shown in Table 2. A deuterium isotope effect of approximately 5 was observed for the deuterated derivatives **37** and **38**. The rate of epimerization increases with pH at about a 10-fold increase per pH unit. The kinetic result is consistent with a hypothesized mechanism of base-catalyzed formation of the achiral enol intermediate leading to racemization of the C-4 chiral center of **20** as well as **21**. By extrapolation, epimers **20** and **21** would have a half-life of approximately 1 year in pH 7.4 buffer. We understand the faster rate of enol formation in the five- and six-membered ring ketones compared to the seven-

membered ring ketones to be the result of the elimination of eclipsing interactions within these ring systems upon enol formation. For the conformationally more flexible seven-membered ring ketone system, enol formation results in greater ring strain thereby leading to a higher energy transition state.

As a 60 nM inhibitor of rat cathepsin K, **20** is approximately 375-fold less potent an inhibitor of this enzyme than of human cathepsin K. The characterization of both cynomolgus monkey²⁴ and rat²⁵ cathepsin K have recently been reported from these laboratories. These studies have shown that mature cathepsin K from cynomolgus monkey is identical to the mature human enzyme. This has permitted the in vivo evaluation of potent inhibitors of human cathepsin K, such as **20**, to determine their ability to inhibit bone resorption in a recently developed medically ovariectomized monkey model of bone turnover. In this model, **20** significantly inhibited bone resorption with once daily subcutaneous dosing at 12 mg/kg as measured by the decrease of the serum bone markers NTx and CTx.²⁶

Alternatively, mature rat cathepsin K has been shown to be 88% identical to the human enzyme.²⁵ Despite the relatively high sequence identity of the rat and human enzymes, their kinetic behavior toward the fluorogenic substrate Cbz-Leu-Arg-aminomethylcoumarin varies considerably (human cathepsin K $K_m = 6$ μ M; rat cathepsin K $K_m = 99$ μ M) with a k_{cat}/K_m 12–35-fold lower for the rat versus the human enzyme. This difference in substrate specificities is also reflected in the significant difference in the potencies of inhibitors such as **20** against the human and rat enzymes. This has precluded the evaluation of many potent inhibitors of human cathepsin K in standard rodent models of bone turnover.⁷ Furthermore, this difference has necessitated the development of separate SARs in order to identify suitably potent inhibitors of rat cathepsin K for evaluation in these models.

Azepanone **24** was identified as an exceptionally potent inhibitor of human cathepsin K ($K_i = 0.0048$ nM) and a sufficiently potent inhibitor of rat cathepsin K to permit in vivo evaluation ($K_{i,app} = 4.8$ nM). The incorporation of the 2-(3-pyridin-2-ylphenyl)acetamide as well as the 5-[2-(4-morpholinyl)ethoxy]-2-benzofuran-2-carboxamide was derived from earlier work in the acyclic 1,3-diaminopropanone series which had shown these functional groups to be favorable for potent inhibition of rat cathepsin K. The potency of **24** versus rat cathepsin K has afforded the opportunity to examine the ability of this inhibitor to attenuate bone resorption in the thyroparathyroidectomized (TPTX) rat as well as bone loss in the ovariectomized (OVX) rat. Continuous intravenous infusion of **24** reduced PTH-induced hypercalcemia in the TPTX rat in a dose-dependent manner. Compound **24** also inhibited bone matrix degradation in the ovariectomized rat.²⁷

Analogue **24** is selective for human cathepsin K versus human cathepsins B, L, and S with $K_{i,app} = 100$, 0.49, and 14 nM, respectively. As with inhibitor **20**, compound **24** has been characterized as a competitive, reversible inhibitor of cathepsin K. Azepanone **24** is a potent inhibitor of native cathepsin K in the osteoclast-mediated bone resorption assay ($IC_{50} = 30$ nM) and in the in situ cytochemical assay, a measure of osteoclast

cathepsin activity ($IC_{50} = 30$ nM). Diastereomer **25** is approximately 1/1000th as potent as **24** versus human cathepsin K with a $K_{i,app} = 4.7$ nM. The precursor, two-component mixture of trans diastereomeric alcohols, **22** inhibited cathepsin K with a $K_{i,app} = 54$ nM confirming the importance of thiol addition to the ketone of the inhibitor as a critical component to the very high potency of **24**. The potency of alcohols **22** is likely the result of the excellent noncovalent interactions at P_3 , P_2 , and P_3' of the inhibitor with critical residues within the active site of the enzyme. In addition, the expected active isomer of alcohols **22** with the *S* configuration at C-4 of the azepanone ring when presenting the amino group as axial would position the C-3 hydroxyl group also in an axial orientation. This relationship has the potential to place the C-3 hydroxyl moiety in the same position as the hydroxyl group of the hemithioacetal of the bound **24** (vide infra). The only difference between the ketone and the alcohol would then be the lack of a covalent bond and the possible introduction of non-bonded sulfur–CH interactions accounting for the 3 orders of magnitude loss of potency between **24** and **22**.

Molecular Modeling and X-ray Crystallography.

1. Predicted Structure of **20 Bound to Cathepsin K.** On the basis of conformational analysis of both diastereomers of the representative model hemithioacetal **39**²⁸ (see also Experimental Section), we developed a representative set of seven azepanone conformers to use in predicting the cathepsin K binding mode of the azepanone scaffold, as part of a structure-based design effort around this structural class. Since this work was initiated prior to separation of the diastereomers, both the *R* and *S* configurations at C-4 were considered. The representative set comprised three conformers of the *R* diastereomer and four conformers of the *S* diastereomer with both axial and equatorial orientations of the C-4 substituent for each diastereomer. Conformational analysis indicates that the equatorial C-4 conformer is favored over the axial conformer with a calculated energy difference of approximately 2 kcal mol⁻¹ (see Experimental Section). This is consistent with the small-molecule crystal structures of both **20** (Figure 2) and **21** (the *R* diastereomer; data not shown).

Each conformer in the representative set was used as a starting point for iterative modeling within the protein active site involving superposition onto related cathepsin K–inhibitor crystal structures.⁶ Despite the preferences seen in small-molecule crystal structures and conformational analysis, modeling within the protein active site led to the prediction of a cathepsin K binding preference for a pseudo-chair conformation of the *S* diastereomer with the C-4 substituent in the higher energy axial orientation (Figure 2).

2. Crystal Structures of **20 and **24** Bound to Cathepsin K.** Initial difficulty in obtaining a cathepsin K co-crystal structure with an azepanone led to the screening of many analogues and both active and inactive diastereomers for co-crystal formation. Ultimately, we obtained crystals of the complex prepared from cathepsin K and the relatively inactive *R* diastereomer **21**. In previous modeling studies it was extremely challenging to develop a plausible binding model for the *R* diastereomer; consistent with these modeling studies, fitting of the *R* diastereomer **21** to the

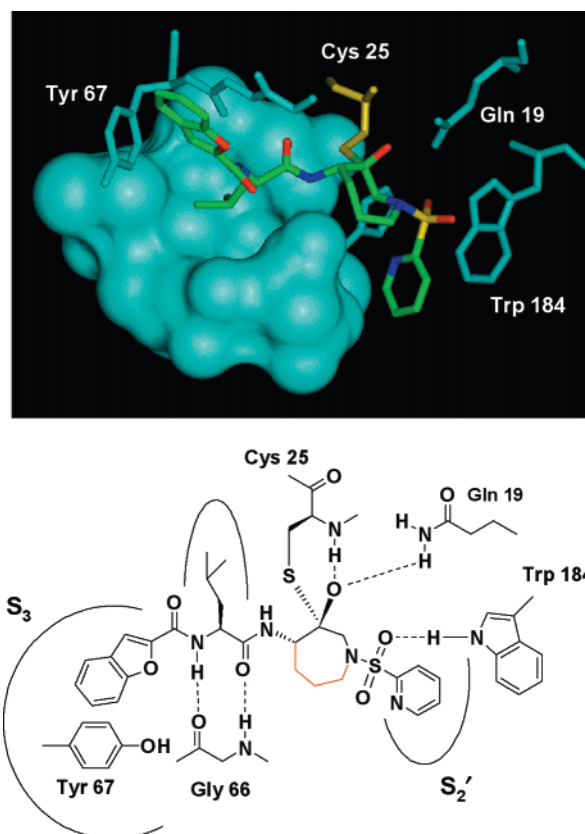


Figure 4. Schematic representations of the 2.0 Å resolution X-ray co-crystal structure of inhibitor **20** bound within the active site of cathepsin K. The inhibitor spans the S_3 to S_2' pockets of the active site of the protein with the thiol of Cys 25 adding to the sterically more congested *Re* face of the carbonyl group of the inhibitor. The C-4 leucinamide group is in an axial orientation off of the azepanone ring which is in a pseudo-chair conformation. The methylene groups of the azepanone ring (highlighted in red) are oriented away from the enzyme toward solvent.

active site during refinement of the crystal structure proved impossible. Inspection of the active site density led to speculation that the bound compound might in fact be the active diastereomer **20**. We tested this hypothesis in an unbiased manner by automated fitting/refinement of our representative set of seven azepanone conformers to the observed active site density. On the basis of visual selection of the conformer that best fit the active site density, an axial conformer of the *S* diastereomer **20** was unambiguously selected as the bound inhibitor.

Preferred binding of the active *S* diastereomer **20** versus the inactive *R* diastereomer **21** is dramatically highlighted by this exclusive crystallographic selection of **20** from a solution of predominantly (96%) **21** during crystal formation and growth. As predicted by the modeling studies, the C-4 leucinamide substituent adopts an axial orientation upon binding to cathepsin K (Figure 6).

The 2.0 Å resolution X-ray co-crystal structure of the inhibitor **20**–cathepsin K complex shows the inhibitor spanning the S_3 – S_2' pockets of the active site of the enzyme (Figure 4). The C-4 leucinamide of **20** is oriented on the unprimed side of the active site with the isobutyl group bound within the hydrophobic S_2 pocket formed by residues Leu 160, Ala 134, and Met 68. The terminal

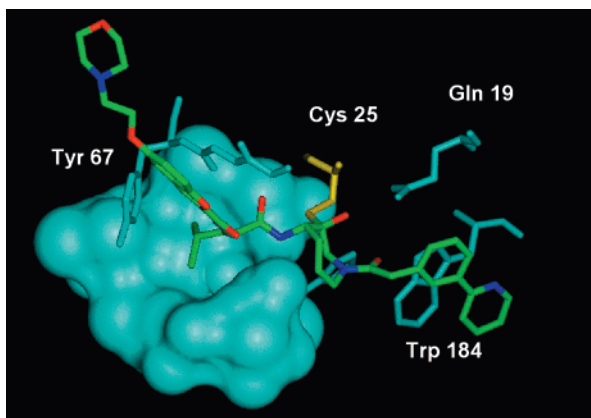


Figure 5. Schematic representations of the 2.8 Å resolution X-ray co-crystal structure of inhibitor **24** bound within the active site of cathepsin K.

benzofuran carboxamide group is bound in the S_3 binding pocket forming an edge-to-face π - π stacking interaction with Tyr 67.²⁹ Two hydrogen bonds are observed between Gly 66 of the enzyme and the leucinamide portion of the inhibitor similar to the antiparallel β -sheet interactions observed in other inhibitor-protease structures.³⁰ As observed in an earlier co-crystal structure of acyclic inhibitor **2** bound within the active site of cathepsin K,^{6a} the 2-pyridyl moiety of **20** occupies the S_2' binding pocket with one of the sulfonamide oxygens forming a hydrogen bond with the indole N-H of Trp 184. The methylene groups of the azepanone ring of **20** are oriented toward solvent (highlighted in red in Figure 4) making no contacts with the protein.

The X-ray co-crystal structure is consistent with the formation of a hemithioketal between Cys 25 of cathepsin K and the carbonyl group of the azepanone, confirming our initial hypothesis for the design of reversible, transition-state inhibitors of cysteine proteases. The thiol of the active site cysteine has added to the diastereotopically more hindered *Re* face of the ketone, syn to the C-4 leucinamide moiety. The oxygen of the resulting hemithioketal is within hydrogen bonding distance of the C(O)NH₂ group of Gln 19 and the N-H of Cys 25.

The 2.8 Å resolution X-ray co-crystal structure of ketone **24** bound within the active site of human cathepsin K (Figure 5) shares most of the features described for the X-ray co-crystal structure of **20**. The co-crystal structure of **24** is consistent with both the *S* stereochemistry and an axial orientation of the leucinamide substituent at the C-4 chiral center as well as hemithioketal formation between the thiol group of the

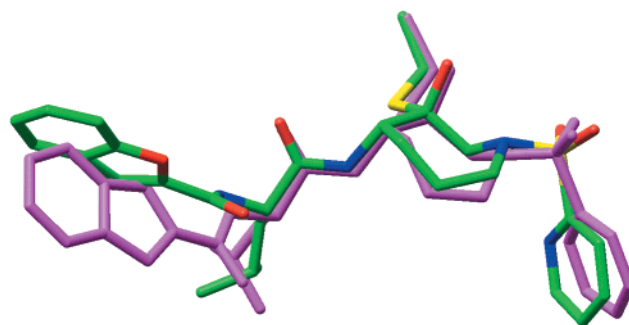
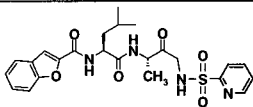
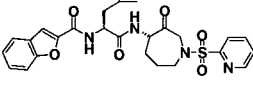
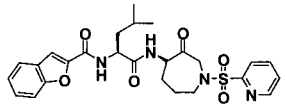
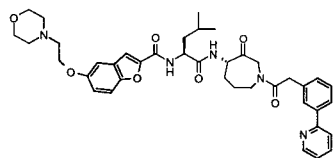
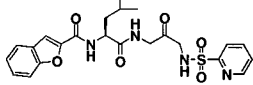
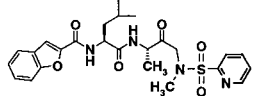


Figure 6. Comparison of the predicted and observed structures of **20** bound to cathepsin K. The conformations and relative positions of several critical active site residues are particularly well-conserved in cathepsin K crystal structures (Gln 19, Cys 25, Trp 26, Tyr 67, His 162, Trp 184; see structures described in ref 6). Heavy-atom superposition of these residues of the enzyme used in modeling onto that observed in the crystal structure yields a close overlap between the predicted binding model (purple) and that observed in the co-crystal structure (color-by-atom). The overlap is especially close for the azepanone rings and proximal parts of the pendant groups. $C\alpha$, $C\beta$, and $S\gamma$ of Cys 25 and the atoms of **20** are shown.

active site Cys 25 and the ketone carbonyl of the inhibitor. In contrast to **20**, inhibitor **24** spans the S_3 - S_3' binding region of the cathepsin K active site with the morpholinoethoxy group extending beyond S_3 , oriented toward solvent. The pyridyl moiety of the 2-(3-pyridin-2-ylphenyl)acetamide extends into the S_3' pocket, forming a face-to-face π - π stacking interaction with Trp 184. The amide oxygen forms a hydrogen bond with the indole N-H of Trp 184, similar to that observed for the sulfonamide oxygen of **20**.

Pharmacokinetic Analysis. Parameters which relate the physicochemical properties of a compound to absorption play a critical role in determining the pharmacokinetics of orally administered drugs.³¹⁻³³ It has been recognized that the oral bioavailability of compounds may also, in part, be a function of enzymatic processes such as metabolism by cytochrome P-450 enzymes and/or transporter efflux mechanisms mediated by P-glycoproteins.³⁴ The configurational stability of the seven-membered ring ketones has allowed us to delineate the effects of inhibitor cyclization as well as the importance of the stereochemistry of the C-4 chiral center in determining the factors which influence the oral bioavailability of these compounds. The pharmacokinetic profiles and efflux properties³⁵ of cyclic analogues **20**, **21**, and **24** as well as the acyclic analogues **2**, **28**, and **36** are presented in Tables 3 and 4. Cyclic analogue **20** showed good oral bioavailability in the rat of 42% with a $T_{1/2}$ of 30 min and a volume of distribution approximately twice that of total body water when dosed orally at 6.3 mg/kg as a solution in 6% aqueous encapsin and 0.5% DMSO. Azepanone **20** was cleared from the systemic circulation at a rate of 50 mL/min/kg. As shown in Table 4, the m-to-s and s-to-m in vitro permeabilities in rat distal colon show **20** to have good membrane permeability and that it is not a substrate for P-glycoprotein transporters as indicated by the similar rates of flux in both the serosal-to-mucosal and mucosal-to-serosal directions. The less potent, C-4 *R* diastereomer **21** was 9.7% orally bioavailable with a $T_{1/2}$ = 33 min and a volume of distribution 1.7 times that of total

Table 3. Pharmacokinetic Properties in the Male Sprague–Dawley Rat

Compound	T _{1/2} (min)	CL (mL/min/kg)	Vd _{ss} (L/kg)	Oral F (%)
 2	33.2	32.5	0.71	3.2
 20	29.8	49.2	1.86	42.1
 21	33.2	51.9	1.64	9.7
 24	338	39.7	1.29	2.1
 28^a	27	33.1	0.65	3.3
 36	21.5	44.6	1.15	2.5

^a Pharmacokinetic properties of analogue **28** were determined in a four-component mixture study format.

Table 4. Oral Bioavailability of Cyclic and Acyclic Analogues as a Function of Physicochemical and Efflux Properties

compd	MW (g/mol)	clog <i>P</i>	H bond donors	H bond acceptors	flux (cm/h)		%F (rat)
					m-to-s	s-to-m	
2	500.6	3.19	3	6	0.011	0.158	3.2
20	526.6	3.08	2	6	0.030	0.084	42.1
21	526.6	3.08	2	6	0.046	0.069	9.7
24	709.8	5.40	2	9	<0.01	0.050	2.1
28	486.5	2.88	3	6	<0.01	0.159	3.3
36	514.6	2.79	2	6	ND	ND	2.5

body water. Diastereomer **21** was cleared at a rate of 52 mL/min/kg. Like **20**, azepanone **21** showed good cell permeability and was not a substrate for apical recycling. The lower oral bioavailability of diastereomer **21** relative to that of diastereomer **20** is therefore likely to be the result of first-pass hepatic and/or intestinal metabolism, perhaps by cytochrome P-450 enzymes. The different inhibitory and pharmacokinetic profiles of diastereomers **20** and **21** highlight the importance of a configurationally stable C-4 chiral center in these analogues.³⁶ The low m-to-s flux but high s-to-m flux of the corresponding acyclic derivatives **2** and **28** (Table 4) shows these analogues to have good cell permeability which are subject to P-glycoprotein-mediated apical recycling, resulting in poor oral bioavailability relative to azepanone **20**. The acyclic *N*-methyl analogue **36**,

which now has the same hydrogen bond donor/acceptor count as **20**, did not lead to an improvement in oral bioavailability.³⁷ The potent rat cathepsin K inhibitor **24** showed poor oral bioavailability with a %F < 2.0%. The low permeability of **24** in the m-to-s direction (<0.01 cm/h) and moderate permeability in the s-to-m direction (0.05 cm/h) suggest that the bioavailability of **24** is likely limited by an apical recycling mechanism and not by poor permeability across membranes.

The s-to-m transport of **2** and **28** is 10–100-fold greater than their m-to-s transport. These results suggest involvement of specific transport mechanism(s) present in the apical membrane of the intestinal epithelial cells which recycle **2** and **28** from the intracellular compartment back into the lumen of the intestine. Therefore, when these cathepsin K inhibitors were added to the mucosal bathing solution, their transepithelial transport appears to be limited by apical recycling. Addition of these cathepsin K inhibitors to the serosal bathing solution results in an apparently greater permeability due to transcellular movement through the cell aided by this apical membrane transporter. Apical recycling has been suggested to be responsible for low bioavailability, increased variability, drug interactions, and the potential for food effects.³⁸

A comparison of the physicochemical properties of azepanone **20** to those of the acyclic derivatives **2**, **28**, and **36** reveals all four analogues to have similar molecular weights (mean MW = 500 g/mol), calculated lipophilicities (mean $\log P = 2.95$), and hydrogen bonding capacities. All three of these parameters fall within the empirically derived values developed by Lipinski and co-workers for estimating solubilities and permeabilities of new chemical entities and suggests that other factors are responsible for determining relative oral bioavailabilities within this set of compounds. As shown in Table 4 and discussed above, the relative oral bioavailabilities of acyclic analogues **2** and **28** compared to the cyclic azepanone **20** appear to be a function of apical recycling from intestinal epithelial cells. One mechanism for apical recycling is the P-glycoprotein (P-gp) efflux pump which is expressed on the luminal surface of intestinal epithelial cells.³⁹ P-Glycoproteins are membrane-bound proteins which are capable of binding a variety of disparate substrates. The drug-binding domains of these enzymes have not yet been fully elucidated, and there has been speculation that several of the postulated transmembrane domains may be involved in substrate recognition. On the basis of the oral bioavailability and efflux properties of these compounds, we suggest that the improved oral bioavailability of azepanone **20** may be the result of the conformational constraint imparted by ring formation effectively locking the rotational freedom of this molecule thereby limiting the number of conformations available for binding to enzymes. From the data presented above it appears that the conformational limitations placed by this specific ring system have locked out those conformations that interact well with those enzyme systems which serve to limit oral bioavailability (i.e. P-gp's) while retaining a bioactive conformation that leads to potent inhibition of the targeted enzyme, cathepsin K. Alternatively, the conformationally flexible acyclic derivatives **2**, **28**, and **36** are postulated to allow access to conformations which are more likely to be substrates for enzyme systems thereby reducing their relative bioavailability.

Conclusions

In this paper we have described the synthesis, in vitro activities, small-molecule and cathepsin K-bound crystal structures, and pharmacokinetic properties of a series of configurationally stable azepanone-based inhibitors of the cysteine protease cathepsin K. Expansion of the five- or six-membered ring ketones to a seven-membered ring has led to a dramatic increase in the configurational stability of the C-4 chiral center contained within these inhibitors. The incorporation of functional groups previously shown to improve in vitro and cell-based potencies in the acyclic 1,3-diaminopropanone series produced potent inhibitors of both human and rat cathepsin K in this azepanone class of compounds. The X-ray co-crystal structures of **20** and **24** bound to cathepsin K confirmed our initial design hypotheses. Molecular modeling studies provided a valid azepanone-binding model in advance of the crystal structure and also provided information crucial to solution of the crystal structure. The increased configurational stability of this class has permitted the examination of the pharmacokinetic, physicochemical, and permeability prop-

erties which are key factors in determining oral bioavailability. These studies have suggested that limiting the rotational freedom of an inhibitor by the introduction of a conformational constraint may serve the dual purpose of locking in a bioactive conformation (thereby leading to potent enzyme inhibition) as well as locking out P-glycoprotein, cytochrome P-450, and other metabolizing enzyme substrate conformations (thereby leading to improved oral bioavailability).

We expect that incorporation of alternative specificity elements into this azepanone template should allow for the selective inhibition of other cysteine proteases while retaining the desirable pharmacokinetic parameters now recognized in this structural class. The inhibitors presented in this paper should serve as excellent compounds for evaluation in both rat and primate models to determine the potential role of cathepsin K inhibition for the treatment of diseases associated with bone loss in humans. These studies will be reported in detail elsewhere.^{26,27}

Experimental Section

General. Except where indicated materials and reagents were used as supplied. Nuclear magnetic resonance spectra were recorded at either 250 or 400 MHz using, respectively, a Bruker AM 250 or Bruker AC 400 spectrometer. Mass spectra were taken on a PE Syx API III instrument using electrospray (ES) ionization techniques. Elemental analyses were obtained using a Perkin-Elmer 240C elemental analyzer. Reactions were monitored by TLC analysis using Analtech silica gel GF or E. Merck silica gel 60 F-254 thin layer plates. Flash chromatography was carried out on E. Merck Kieselgel 60 (230–400 mesh) silica gel.

Allylpent-4-enylcarbamic Acid Benzyl Ester (8). To a suspension of NaH (1.83 g, 76.33 mmol of 90% NaH) in DMF was added benzyl *N*-allyl-*N*-1-pentenylcarbamate (7.3 g, 38.2 mmol) in a dropwise fashion. The mixture was stirred at room temperature for 10 min whereupon 5-bromo-1-pentene (6.78 mL, 57.24 mmol) was added in a dropwise fashion. The reaction was heated to 40 °C for approximately 4 h whereupon it was partitioned between dichloromethane and water. The organic layer was washed with water (2 \times), brine, dried (MgSO₄), filtered and concentrated. Column chromatography of the residue (10% ethyl acetate:hexanes) provided 10.3 g (104%) of **8** as an oil: ¹H NMR (400 MHz, CDCl₃) δ 7.3–7.4 (m, 5H), 5.8 (m, 2H), 5.4 (m, 4H), 5.0 (m, 2H), 3.8 (m, 2H), 3.4 (m, 2H), 2.1 (m, 2H), 1.7 (m, 2H); MS (ESI) 260 (M + H)⁺.

2,3,4,7-Tetrahydroazepine-1-carboxylic Acid Benzyl Ester (9). To a degassed solution of diene **8** (50 g, 192 mmol) in CH₂Cl₂ was added bis(tricyclohexylphosphine)benzylidineruthenium(IV)dichloride (5.0 g, 6.1 mmol). The reaction was heated to reflux until complete consumption of the starting material was observed by TLC analysis. The mixture was concentrated and chromatographed (1:1 CH₂Cl₂:hexanes) to provide 35 g (70%) of azepine **9** as a brown oil: ¹H NMR (400 MHz, CDCl₃) δ 7.3 (m, 5H), 5.7 (m, 2H), 5.1 (m, 2H), 4.0 (dd, 2H), 3.6 (m, 2H), 2.2 (m, 2H), 1.7 (m, 2H); MS (ESI) 232 (M + H)⁺. Anal. (C₁₆H₂₁N₄O₂) C, H, N.

8-Oxo-3-azabicyclo[5.1.0]octane-3-carboxylic Acid Benzyl Ester (10). To a 5 °C solution of **9** (39 g, 168 mmol) in CH₂Cl₂ (1.2 L) was added *m*-CPBA (55 g) in a portionwise manner. Upon complete addition the mixture was maintained at 5 °C for 15 min. The mixture was then stirred at room temperature overnight. The following day dimethyl sulfide (3 mL) was added and the mixture maintained at room temperature for 1 h. This mixture was filtered and concentrated. The residue was dissolved in EtOAc and washed with 10% K₂CO₃ (3 \times), brine (3 \times), dried (Na₂SO₄), filtered and concentrated to provide 39 g (94%) of the crude epoxide **10**. This material was of sufficient purity to carry on to the following reaction with no further purification: ¹H NMR (400 MHz, CDCl₃) δ 7.4 (m

5H), 5.2 (s, 2H), 4.1 (m, 1H), 3.6 (m, 2H), 3.2 (m, 2H), 2.9 (m, 1H), 2.1 (m, 1H), 1.9 (m, 1H), 1.7 (m, 2H); MS (ESI) 248 (M + H)⁺.

4(*R,S*)-Azido-3(*R,S*)-hydroxyazepane-1-carboxylic Acid Benzyl Ester (11). To a solution of the epoxide **10** (2.0 g, 8.1 mmol) in methanol:water (8:1 solution) were added NH₄Cl (1.3 g, 24.3 mmol) and sodium azide (1.6 g, 24.3 mmol). The reaction was heated to 70 °C until complete consumption of the starting epoxide was observed by TLC analysis. The majority of the solvent was removed in vacuo and the remaining solution was partitioned between ethyl acetate and pH 4 buffer. The organic layer was washed with saturated NaHCO₃, water, and brine, dried (MgSO₄), filtered, and concentrated. Column chromatography (20% ethyl acetate:hexanes) of the residue provided 1.3 g (55%) of **11**: ¹H NMR (400 MHz, CDCl₃) δ 8.0 (s, 1H), 7.4 (m, 5H), 5.2 (s, 2H), 4.0 (m, 1H), 3.6 (m, 2H), 3.2 (m, 1H), 3.0 (m, 2H), 2.2 (m, 1H), 2.0 (m, 1H), 1.7 (m, 2H); MS (ESI) 291 (M + H)⁺.

4(*R,S*)-Amino-3(*R,S*)-hydroxyazepane-1-carboxylic Acid Benzyl Ester (13). To a solution of **11** and **12** (12.3 g, 42.5 mmol) in methanol (400 mL) were added triethylamine (17.8 mL, 127.4 mmol) and 1,3-propanedithiol (12.8 mL, 127.4 mmol). The reaction was maintained at room temperature until complete consumption of the starting material was observed as determined by TLC analysis. The reaction was concentrated and chromatographed (20% methanol:ethyl acetate) to provide 6.8 g (61%) of amino alcohol **13** as a clear viscous oil: ¹H NMR (400 MHz, CDCl₃) δ 7.3 (m, 5H), 5.1 (m, 2H), 3.7 (m, 1H), 3.4 (s, 1H), 3.3 (m, 2H), 3.0 (m, 1H), 2.6 (m, 1H), 2.4 (b, 2H), 1.9 (m, 2H), 1.7 (m, 1H), 1.4 (m, 1H); MS (ESI) 265 (M + H)⁺. Anal. (C₁₆H₂₁N₃O₂) C, H, N.

(*S*)-1-[1-[4(*R,S*)-((*S*)-2-Benzylloxycarbonylamino-4-methylpentanoylamino)-3(*R,S*)-hydroxyazepan-1-yl]-methanoyl]-3-methylbutyl carbamic Acid Benzyl Ester (14). To a solution of the amino alcohol **13** (3.0 g, 11.3 mmol) in CH₃OH (25 mL) was added 10% Pd/C (0.03 g). The mixture was shaken under 35 psi of hydrogen for approximately 5 h whereupon it was filtered through Celite. The filter cake was washed several times with CH₃OH and CH₂Cl₂. Concentration of the filtrate provided 0.67 g (46%) of 4(*R,S*)-aminoazepan-3(*R,S*)-ol as a clear oil: ¹H NMR (400 MHz, CD₃OD, reported as a mixture of diastereomers) δ 3.31–3.30 (m, 3H), 3.01–2.69 (m, 6H), 1.82–1.56 (m, 5H); MS (ESI) 131.2 (M + H)⁺.

To a solution of 4(*R,S*)-aminoazepan-3(*R,S*)-ol (0.67 g, 5.13 mmol) in CH₂Cl₂ (30 mL) were added EDC (2.17 g, 11.33 mmol) and Cbz-leucine (2.74 g, 10.30 mmol). The reaction was maintained at room temperature until complete consumption of the starting material was observed by TLC analysis. The mixture was concentrated, diluted with EtOAc and washed with saturated K₂CO₃, 1 N HCl, brine, dried (MgSO₄) filtered and concentrated. Column chromatography of the residue (4:1 EtOAc:hexanes) provided 1.4 g (44%) of alcohols **14** as a white powder: MS (ESI) 625.3 (M + H)⁺, 644.3 (M + Na)⁺.

(*S*)-1-[1-[4(*R,S*)-((*S*)-2-Benzylloxycarbonylamino-4-methylpentanoylamino)-3-oxoazepan-1-yl]methanoyl]-3-methylbutyl carbamic Acid Benzyl Ester (15 and 16). To a solution of the alcohols **14** (0.20 g, 0.32 mmol) in CH₂Cl₂ (5.0 mL) was added Dess–Martin periodinane (0.27 g, 0.64 mmol). The mixture was maintained at room temperature for 30 min whereupon saturated NaHCO₃ and 10% Na₂S₂O₃ were added. The aqueous layer was extracted with CH₂Cl₂. The combined organic layers were dried (MgSO₄), filtered and concentrated. Column chromatography (2:1 EtOAc:hexanes) provided 0.16 g (83%) of **6** as a white solid. Separation of this mixture by preparative HPLC provided the faster eluting diastereomer **15** (t_R = 16.9 min; >98% purity): MS (ESI) 623.3 (M + H)⁺. Anal. (C₃₄H₄₆N₄O₇·0.4H₂O) C, H, N, O. And the slower eluting diastereomer **16** (t_R = 21.8 min; >96% purity): MS (ESI) 623.1 (M + H)⁺. Anal. (C₃₄H₄₆N₄O₇·0.3H₂O) C, H, N, O.

4(*R,S*)-[(*S*)-1-(3(*R,S*)-Hydroxyazepan-4-ylcarbonyl)-3-methylbutyl]carbamic Acid *tert*-Butyl Ester (17). To a solution of the amino alcohol **13** (0.72 g, 2.72 mmol) in CH₂Cl₂ were added EDC (0.52 g), HOBt (0.37 g) and *N*-Boc-

leucine (0.63 g). The reaction was maintained at room temperature until complete consumption of the starting material was observed by TLC analysis. The reaction was diluted with ethyl acetate and washed with 1 N HCl, saturated K₂CO₃, water, brine, dried (MgSO₄), filtered and concentrated. Column chromatography of the residue (3% methanol:dichloromethane) gave 1.0 g (77%) of 4(*R,S*)-((*S*)-2-*tert*-butoxycarbonylamino-4-methylpentanoylamino)-3(*R,S*)-hydroxyazepan-1-carboxylic acid benzyl ester: ¹H NMR (400 MHz, CDCl₃, reported as a mixture of diastereomers) 7.35 (m, 5H), 6.7 (bs, 1H), 5.15 (m, 3H), 4.0–3.0 (m, 10H), 2.0–1.7 (m, 5H), 1.4 (s, 9H), 0.9 (m, 6H); MS (ESI) 478 (M + H)⁺.

To a solution of 4(*R,S*)-((*S*)-2-*tert*-butoxycarbonylamino-4-methylpentanoylamino)-3(*R,S*)-hydroxyazepan-1-carboxylic acid benzyl ester (18.0 g, 37.7 mmol) and 10% Pd/C (catalytic) in ethyl acetate:methanol (300 mL of a 2:1 solution) was affixed a balloon of hydrogen. The reaction was stirred until complete consumption of the starting material was observed by TLC analysis. The reaction was filtered to remove the catalyst and the filtrate was concentrated to provide 12.6 g (97%) of **17** as a white powder: ¹H NMR (400 MHz, CDCl₃, reported as a mixture of diastereomers) δ 5.5 (br s, 1H), 5.2 (br s, 1H), 4.1 (m, 1H), 4.0 (m, 1H), 3.75 (m, 3H), 3.1 (m, 2H), 2.9 (m, 1H), 1.7 (m, 5H), 1.45 (s, 9H), 0.9 (m, 6H); MS (ESI) 344 (M + H)⁺.

4(*R,S*)-Benzofuran-2-carboxylic Acid 4-[(*S*)-3-Methyl-1-[3(*R,S*)-hydroxy-1-(pyridin-2-ylsulfonyl)azepan-4-ylcarbonyl]butyl]amide (18). To a solution of amine **17** (12 g, 34.9 mmol) in CH₂Cl₂ was added triethylamine (5.8 mL, 41.9 mmol) followed by the dropwise addition of 2-pyridine-sulfonyl chloride (7.4 g, 41.9 mmol). The reaction was stirred until complete as determined by TLC analysis. The mixture was washed with saturated NaHCO₃, water, brine, dried (Na₂SO₄), filtered and concentrated. Column chromatography (75% ethyl acetate:hexanes to 100% ethyl acetate) of the residue provided 15 g (88%) of 4(*R,S*)-[(*S*)-1-[3(*R,S*)-hydroxy-1-(pyridin-2-ylsulfonyl)azepan-4-ylcarbonyl]-3-methylbutyl]carbamic acid *tert*-butyl ester: MS (ESI) 484 (M + H)⁺.

To a solution of 4(*R,S*)-[(*S*)-1-[3(*R,S*)-hydroxy-1-(pyridin-2-ylsulfonyl)azepan-4-ylcarbonyl]-3-methylbutyl]carbamic acid *tert*-butyl ester (15.7 g, 32.4 mmol) in CH₃OH (50 mL) was added 4 M HCl in dioxane (50 mL). The reaction was maintained at room temperature until complete consumption of the starting material was observed. The mixture was concentrated to provide 13.7 g (100%) of 4(*R,S*)-[(*S*)-2-amino-4-methylpentanoic acid [3(*R,S*)-hydroxy-1-(pyridin-2-ylsulfonyl)azepan-4-yl]amide hydrochloride as a white powder: MS (ESI) 385 (M + H)⁺.

To a solution of 4(*R,S*)-[(*S*)-2-amino-4-methylpentanoic acid [3(*R,S*)-hydroxy-1-(pyridin-2-ylsulfonyl)azepan-4-yl]amide hydrochloride (8.7 g, 20.7 mmol) in CH₂Cl₂ (50 mL) were added EDC (4.0 g, 20.9 mmol), HOBt (2.5 g, 19.0 mmol), TEA (5.3 mL, 37.9 mmol) and benzofuran-2-carboxylic acid (3.4 g, 20.9 mmol). The mixture was maintained at room temperature until complete consumption of the starting material was observed as determined by TLC analysis. The mixture was concentrated, diluted with EtOAc and washed with 1 N HCl, saturated K₂CO₃, H₂O, brine, dried (MgSO₄), filtered and concentrated. Column chromatography of the residue provided 10 g (91%) of **18** as a white powder: ¹H NMR (400 MHz, CDCl₃, reported as a mixture of diastereomers) δ 8.7 (m, 1H), 8.0 (m, 2H), 7.6 (m, 1H), 7.4 (m, 4H), 7.2–7.3 (m, 3H), 5.0 (m, 1H), 4.7 (m, 2H), 4.0 (m, 1H), 3.7 (dd, 1H), 2.7 (m, 1H), 2.2 (m, 2H), 1.5–2.1 (m, 5H), 1.0 (m, 6H); MS (ESI) 529 (M + H)⁺.

4(*R,S*)-Benzofuran-2-carboxylic Acid [(*S*)-3-Methyl-1-[3-oxo-1-(pyridin-2-ylsulfonyl)azepan-4-ylcarbonyl]-butyl]amide (19). To a solution of alcohols **18** (10 g, 18.8 mmol) in DMSO (20 mL) were added TEA (10.5 mL, 75.7 mmol) and pyridine sulfur trioxide complex (6.02 g, 37.8 mmol). The mixture was maintained at room temperature for approximately 2 h whereupon it was diluted with EtOAc and washed with H₂O, brine, dried (MgSO₄), filtered and concentrated. Column chromatography (3% CH₃OH/CH₂Cl₂) provided 8.2 g (81%) of the ketones **19** as a 1:1 mixture of diastereomers as determined by analytical HPLC (Chiralpak AD; 4.6 × 250

mm; 10 μ m; 100% CH₃CN; 1 mL/min flow rate with UV detection at 254 nm). Preparative HPLC separation of the mixture **19** (Chiralpak AD; 50 \times 250 mm; 20 μ m; 100% CH₃CN; 108 mL/min flow rate with UV detection at 320 nm) provided the faster eluting diastereomer **20** (t_R = 5.6 min, >95% purity): ¹H NMR (DMSO-*d*₆, 400 MHz) 8.74 (d, 1H), 8.60 (d, 1H), 8.33 (d, 1H), 8.11 (t, 1H), 7.97 (d, 1H), 7.77 (d, 1H), 7.71–7.66 (m, 2H), 7.62 (s, 1H), 7.46 (t, 1H), 7.33 (t, 1H), 4.80 (m, 1H), 4.59 (m, 1H), 4.36 (d, 1H), 3.86 (m, 2H), 2.86 (m, 1H), 1.88–1.57 (m, 7H), 0.92 (m, 6H); MS (ESI) 527 (M + H⁺, 100%). Anal. (C₂₆H₃₀N₄O₆S) C, H, N, S. And the slower eluting diastereomer **21** (t_R = 9.9 min, >95% purity): MS (ESI) 527 (M + H⁺, 100%). Anal. (C₂₆H₃₀N₄O₆S) C, H, N, S.

4(R,S)-5-(2-Morpholin-4-ylethoxy)benzofuran-2-carboxylic Acid ((S)-3-Methyl-1-{3(R,S)-hydroxy-1-[2-(3-pyridin-2-ylphenyl)acetyl]azepan-4-ylcarbamoyl}butyl)amide (22). To a solution of amino alcohol **17** (10.0 g, 29.1 mmol) in CH₂Cl₂ (200 mL) were added HOBt (4.32 g, 32.0 mmol), EDC (6.14 g, 32.0 mmol) and 2-(3-pyridin-2-ylphenyl)acetic acid (4.23 g, 32.0 mmol). The reaction was maintained at room temperature until complete consumption of the starting material was observed. The mixture was washed with H₂O, saturated NaHCO₃ and brine. The organic layer was dried (MgSO₄), filtered and concentrated. Column chromatography (5% CH₃OH:CH₂Cl₂) of the residue provided 13.6 g (86%) of 4(R,S)-((S)-1-{3(R,S)-hydroxy-1-[2-(3-pyridin-2-ylphenyl)ethanoyl]azepan-4-ylcarbamoyl}-3-methylbutyl)carbamoyl}butyl ester as a white foam: MS (ESI) 539 (M + H⁺).

To a solution of 4(R,S)-((S)-1-{3(R,S)-hydroxy-1-[2-(3-pyridin-2-ylphenyl)ethanoyl]azepan-4-ylcarbamoyl}-3-methylbutyl)carbamoyl}butyl ester (13.0 g, 24.0 mmol) in methanol (100 mL) was added 4 M HCl in dioxane (100 mL). The mixture was stirred until complete consumption of the starting material was observed as determined by TLC analysis. The mixture was concentrated in vacuo to provide 10.5 g (85%) of 4(R,S)-((S)-2-amino-4-methylpentanoic acid {3(R,S)-hydroxy-1-[2-(3-pyridin-2-ylphenyl)ethanoyl]azepan-4-yl}amide hydrochloride as a white powder: MS (ESI) 439 (M + H⁺).

To a solution of the 4(R,S)-((S)-2-amino-4-methylpentanoic acid {3-hydroxy-1-[2-(3-pyridin-2-ylphenyl)ethanoyl]azepan-4-yl}amide hydrochloride (9.0 g, 17.6 mmol) in CH₂Cl₂ (150 mL) were added HOBt (2.4 g, 17.6 mmol), EDC (3.4 g, 17.6 mmol) and 5-[2-(4-morpholinyl)ethoxy]-2-benzofuran-2-carboxylic acid (5.12 g, 17.6 mmol). The mixture was maintained at room temperature until complete consumption of the starting material was observed by TLC analysis. Standard workup and column chromatography (10% CH₃OH:CH₂Cl₂) provided 13.4 g (91%) of alcohols **22** as a white foam: MS (ESI) 712 (M + H⁺).

4(R,S)-5-(2-Morpholin-4-ylethoxy)benzofuran-2-carboxylic Acid ((S)-3-Methyl-1-{3-oxo-1-[2-(3-pyridin-2-ylphenyl)acetyl]azepan-4-ylcarbamoyl}butyl)amide (23). To a solution of alcohols **22** (13.0 g, 18.3 mmol) in DMSO (200 mL) were added triethylamine (7.60 mL, 54.8 mmol) and pyridine sulfur trioxide complex (8.72 g, 54.8 mmol). The mixture was maintained at room temperature for approximately 2 h whereupon it was diluted with EtOAc and washed with H₂O, brine, dried (MgSO₄), filtered and concentrated. Column chromatography (5% CH₃OH:CH₂Cl₂) of the residue provided 8.9 g (68%) of ketones **23** as a 1:1 mixture of diastereomers as determined by analytical HPLC (Whelk O-1 (R,R); 4.6 \times 250 mm; 10 μ m; 100% CH₃OH with 50 mM NH₄OAc; 1 mL/min flow rate with UV detection at 254 nm). Preparative HPLC separation of the diastereomers **23** (Whelk O-1 (R,R); 21.2 \times 250 mm; 10 μ m; 100% CH₃OH with 50 mM NH₄OAc; 20 mL/min flow rate with UV detection at 335 nm) provided the faster eluting diastereomer **24** (t_R = 9.2 min, >97% purity by HPLC analysis) and the slower eluting diastereomer **25** (t_R = 10.4 min, >95% purity by HPLC analysis).

5-(2-Morpholin-4-ylethoxy)benzofuran-2-carboxylic Acid ((S)-3-Methyl-1-{(S)-3-oxo-1-[2-(3-pyridin-2-ylphenyl)acetyl]azepan-4-ylcarbamoyl}butyl)amide (24). Anal. (C₄₀H₄₇N₅O₇·0.35H₂O) C, H, N.

5-(2-Morpholin-4-ylethoxy)benzofuran-2-carboxylic Acid ((S)-3-Methyl-1-{(R)-3-oxo-1-[2-(3-pyridin-2-ylphenyl)acetyl]azepan-4-ylcarbamoyl}butyl)amide (25). Anal. (C₄₀H₄₇N₅O₇·1.4H₂O) C, H, N.

{(S)-1-[Hydroxy-3-(pyridin-2-ylsulfonylamino)propylcarbamoyl]-3-methylbutyl}carbamoyl}butyl ester *tert*-Butyl Ester (27). To a solution of 1,3-diamino-2-hydroxypropane **26** (3.37 g, 37.5 mmol) in DMF (65 mL) were added *N*-Boc-L-leucine (9.34 g, 37.5 mmol), HOBt (5.5 g, 40.7 mmol) and EDC (7.77 g, 40.7 mmol). The mixture was maintained at room temperature until complete consumption of the starting material was observed as determined by TLC analysis. The mixture was diluted with EtOAc and washed with water, brine, dried, filtered and concentrated. To a solution of the residue in CH₂Cl₂ were added NMM (4.4 mL, 140 mmol) and 2-pyridinesulfonyl chloride (3.7 g, 20.84 mmol) and maintained at room temperature for 2 h. Workup and column chromatography (1:1 EtOAc:hexanes to 100% EtOAc) provided 4.3 g (25%) of alcohol **27** as a white foam: ¹H NMR (400 MHz, CDCl₃) δ 8.70 (d, 1H), 8.03 (d, 1H), 7.94 (t, 1H), 7.52 (dd, 1H), 7.14 (m, 1H), 6.51 (m, 1H), 5.48–5.33 (m, 1H), 3.84 (m, 1H), 3.54–3.11 (m, 5H), 1.68–1.49 (m, 5H) 1.40 (s, 9H), 0.92 (m, 6H).

Benzofuran-2-carboxylic Acid {(S)-3-Methyl-1-[2-oxo-3-(pyridin-2-ylsulfonylamino)propylcarbamoyl]butyl}amide (28). To a solution of **27** (2.1 g, 4.73 mmol) in CH₂Cl₂ (30 mL) was added TFA (30 mL). This mixture was maintained at room temperature for 2 h whereupon it was concentrated. The residue was azeotroped with CH₂Cl₂ (2 \times), toluene (2 \times), washed with ether (2 \times) and filtered to provide 2.1 g of the TFA amine salt as a white powder. This material was of sufficient purity to carry on to the next step with no further purification.

To a solution of the amine salt (0.4 g, 0.87 mmol) in DMF (4 mL) was added benzofuran-2-carboxylic acid (0.11 g, 0.7 mmol), NMM (0.3 mL, 2.8 mmol) and HBTU (0.27 g, 0.7 mmol). The mixture was maintained at room temperature for 3 h whereupon it was diluted with EtOAc and washed with water, brine, dried, filtered and concentrated. Column chromatography (5% CH₃OH:CH₂Cl₂) of the residue provided 0.42 g (71%) of benzofuran-2-carboxylic acid {(S)-3-methyl-1-[2-hydroxy-3-(pyridin-2-ylsulfonylamino)propylcarbamoyl]butyl}amide as a white foam: ¹H NMR (400 MHz, CDCl₃) δ 8.58 (m, 1H), 7.90 (m, 1H), 7.77 (m, 1H), 7.61 (m, 1H), 7.48–7.23 (m, 6H), 6.45 (m, 1H), 4.71 (m, 1H), 3.95 (m, 1H), 3.54–3.08 (m, 5H), 1.75 (m, 4H), 0.93 (m, 6H); MS (ESI) 489.2 (M + H⁺).

To a solution of benzofuran-2-carboxylic acid {(S)-3-methyl-1-[2-hydroxy-3-(pyridin-2-ylsulfonylamino)propylcarbamoyl]butyl}amide (0.3 g, 0.61 mmol) in CH₂Cl₂ (5.0 mL) was added Dess–Martin periodinane (0.5 g, 1.18 mmol). The mixture was maintained at room temperature for approximately 2 h whereupon saturated Na₂S₂O₃ and saturated NaHCO₃ were added and the mixture stirred for 10 min. Workup and column chromatography (70% EtOAc:30% hexanes) provided 0.12 g which was further purified by HPLC to provide 0.048 g (8%) of ketone **28** as a white foam: ¹H NMR (400 MHz, CDCl₃) δ 8.63 (d, 1H), 7.93 (d, 1H), 7.84 (t, 1H), 7.66 (d, 1H), 7.51–7.18 (m, 6H), 6.06 (br s, 1H), 4.77 (m, 1H), 4.21 (m, 4H), 1.82–1.75 (m, 4H), 0.98 (m, 6H); MS (ESI) 487.2 (M + H⁺). Anal. (C₂₃H₂₆N₄O₆S·1.1H₂O) C, H, N.

Crystallization of the Complex of Cathepsin K with Inhibitor 24. Crystals of mature activated cathepsin K complexed with the inhibitor were grown by the vapor diffusion method from a solution of 10% PEG 8000, 0.1 M imidazole pH 8.0 and 0.2 M calcium acetate. Crystals of the complex are orthorhombic, space group *P*2₁2₁2₁, with cell constants *a* = 71.8 Å, *b* = 75.9 Å and *c* = 114.8 Å. The structure was determined by molecular replacement with a model consisting of all protein atoms from the previously determined cathepsin K/E-64 complex.⁴⁰ The structure was refined at 2.8 Å resolution. The final *R*_c was 0.260.

Crystallization of the Complex of Cathepsin K with Inhibitor 20. Crystals of mature activated cathepsin K complexed with the inhibitor were grown by the vapor diffusion method from a solution of 30% MPD, 0.1 M MES pH 7.0, 0.1

M tris buffer at pH 7.0 and 90 mM DTT. Crystals of the complex are tetragonal, space group $P4_3$, with cell constants $a = 100.9 \text{ \AA}$ and $c = 53.7 \text{ \AA}$. The structure was determined as described above and refined at 2.0 \AA . The final R_c was 0.263.

Molecular Modeling. Model building and conformational searches were performed with MacroModel⁴¹ in the context of the MMFF⁴² with the GB/SA solvent model.⁴³ Applying energy and conformational difference (based on visual inspection of superimposed conformers) as selection criteria, seven conformers were chosen as representative of the low energy structures observed in the two searches. Both diastereomers were represented, and based on inspection of crystal structures of related complexes, conformers with equatorial and axial peptide were selected. The models were superimposed into the active sites of cathepsin K complexes of the related compounds, and then visually inspected for goodness-of-fit to the cathepsin K active site, which proved especially critical on the unprime side of the active site. Models that formed good interactions with the enzyme were used as starting points for elaboration of the complete inhibitor from the model structure. This procedure, in conjunction with manual adjustment of the initial and progressive binding models, led to the unambiguous selection of a binding model based on an axial conformer of **20**. The selected conformer of the model compound allowed for straightforward elaboration to the full inhibitor in the active site, and satisfied several key interactions with the enzyme. Model elaboration from other starting points proved unproductive, although in some cases extensive manual adjustment ultimately yielded a binding conformation very similar to that obtained from simple extension of the selected model.

Mass Spectral Analysis of Cathepsin K–Inhibitor Complexes. The inhibitor, dissolved in DMSO, was diluted in water (Milli-Q 18 M Ω) to a molar concentration 5-fold that of the enzyme, with a 20% final volume of DMSO making sure that the inhibitor was completely dissolved. Human cathepsin K was provided in buffer (100 mM sodium acetate, 100 mM NaCl, 2 mM l-cysteine pH 5.5). An aliquot containing 1 nmol of the enzyme was mixed 1:1 with inhibitor solution in a 0.65-mL plastic centrifuge tube, vortexed, and a minimum of 120-min incubation time was allowed before analysis by LC–ESIMS. The entire reaction mixture was injected onto a peptide trap and the trap washed with 1 mL of water (Milli-Q 18 M Ω) manually before being back eluted onto the analytical column.

Kinetic Study of Epimerization. The rates of epimerization were determined by HPLC analysis utilizing a MetaChem Inertsil ODS-3, 5 μm , 250 \times 4.6 mm; eluent: 1/1 acetonitrile/20 mM pH 7.0 phosphate buffer; flow rate, 1 mL/min; detection, UV at 215 and 254 nm. Each compound was initially prepared in DMSO as a 10 mM stock solution. An appropriate volume of the stock was diluted into the aqueous buffer, pH ranging from 7 to 12.5, at the final concentration of 50 μM . 20- μL aliquots of the resulting solution were withdrawn at designated elapsed times and immediately injected into the HPLC for analysis. For all compounds tested, the epimerization rates were negligible at pH 7, the injection of the test solution into the HPLC eluent, which was 50/50 acetonitrile/pH 7 buffer, essentially stopped the reaction. With the assumption of a first-order kinetics and a final 1:1 equilibrium concentration ratio, the epimerization rate constant k can be determined based on the following equation: $A(t)/A(0) = (e^{-kt} + 1)/2$, where $A(0)$ and $A(t)$ are chromatographic peak areas at time = 0 and t , respectively.

Pharmacokinetic Analysis. Animal procedures reported in these studies were approved by the Animal Care and Use Committee at SmithKline Beecham Pharmaceuticals. All dosages were prepared as solutions in water with up to 20% encapsin and up to 3% DMSO. Previous experience with the vehicles has shown them to have minimal effect on pharmacokinetics in the rat. Studies were conducted in a crossover fashion on 2 separate days, 2 days apart. On study day 1 rats received a 30-min intravenous infusion of the test compound, and on study day 2, the same rats received an oral bolus gavage of the same compound. All compounds except **28** were

dosed as single components (**28** was dosed as a mixture of 4 compounds). Blood samples were obtained from a lateral tail vein and plasma isolated by centrifugation. Plasma concentrations of test compounds were quantified by liquid chromatography/tandem mass spectroscopy, with lower limits of quantitation of 5–10 ng/mL. Standard data analysis techniques were used to derive pharmacokinetic parameters from the plasma concentration versus time data.⁴⁴

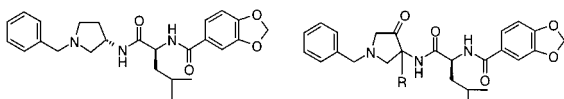
Acknowledgment. The authors thank Drs. John Gleason and Brian Metcalf for their support of this work.

Supporting Information Available: Synthesis and characterization of inhibitors **2** and **36** and X-ray crystallographic data for **20**. This material is available free of charge via the Internet at <http://pubs.acs.org>.

References

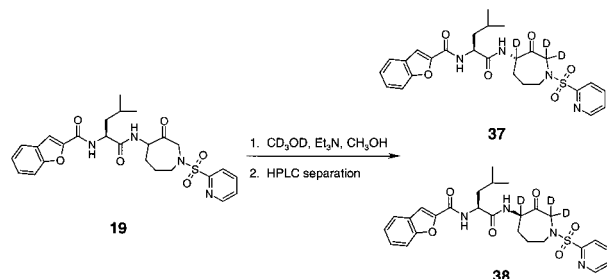
- (1) (a) Drake, F. H.; Dodds, R. A.; James, I. A.; Connor, J. R.; Debouck, C.; Richardson, S.; Lee-Ryckaczewski, L.; Coleman, L.; Riemann, D.; Barthlow, R.; Hastings, G.; Gowen, M. Cathepsin K, but not cathepsins B, L or S is abundantly expressed in human osteoclasts. *J. Biol. Chem.* **1996**, *271*, 12511–12516. (b) Brömme, D.; Okamoto, K. Human cathepsin O2, a novel cysteine protease highly expressed in osteoclastomas and ovary. Molecular cloning, sequencing and tissue distribution. *Biol. Chem. Hoppe-Seyler* **1995**, *376*, 379–384. (c) Shi, G.-P.; Chapman, H. A.; Bhairi, S. M.; DeLeeuw, C.; Reddy, V. Y.; Weiss, S. J. Molecular cloning of human cathepsin O, a novel endoproteinase and homologue of rabbit OC2. *FEBS Lett.* **1995**, *357*, 129–134. (d) Littlewood-Evans, A.; Kokubo, T.; Ishibashi, O.; Inaoka, T.; Wlodarski, B.; Gallagher, J. A.; Bilbe, G. Localization of cathepsin K in human osteoclasts by *in situ* hybridization and immunohistochemistry. *Bone* **1997**, *20*, 81–86. (e) Bossard, M. J.; Tomaszek, T. A.; Thompson, S. K.; Amegadzie, B. Y.; Hanning, C. R.; Jones, C.; Kurdyla, J. T.; McNulty, D. E.; Drake, F. H.; Gowen, M.; Levy, M. A. Proteolytic activity of human osteoclast cathepsin K. Expression, activation, and substrate identification. *J. Biol. Chem.* **1996**, *271*, 12517–12524.
- (2) Inui, T.; Ishibashi, O.; Inaoka, T.; Origane, Y.; Kumegawa, M.; Kokubo, T.; Yamaura, T. Cathepsin K antisense oligodeoxynucleotide inhibits osteoclastic bone resorption. *J. Biol. Chem.* **1997**, *272*, 8109–8112.
- (3) (a) Saftig, P.; Hunziker, E.; Wehmeyer, O.; Jones, S.; Boyde, A.; Rommerskirch, W.; Detlev, J. D.; Schu, P.; von Figura, K. Impaired osteoclastic bone resorption leads to osteopetrosis in cathepsin K deficient mice. *Proc. Natl. Acad. Sci. U.S.A.* **1998**, *95*, 13453–13458. (b) Gowen, M.; Lazner, F.; Dodds, R.; Kapadia, R.; Feild, J.; Tavaría, M.; Bertoncello, I.; Drake, F.; Zavorselk, S.; Tellis, I.; Hertzog, P.; Debouck, C.; Kola, I. Cathepsin K knockout mice develop osteopetrosis due to a deficit in matrix degradation but not demineralization. *J. Bone Miner. Res.* **1999**, *14*, 1654–1663.
- (4) (a) Gelb, B. D.; Moissoglu, K.; Zhang, J.; Martignetti, J. A.; Bromme, D.; Desnick, R. J. Cathepsin K; isolation and characterization of the murine cDNA and genomic sequence, the homologue of the human pycnodysostosis gene. *Biochem. Mol. Med.* **1996**, *59*, 200–206. (b) Johnson, M. R.; Polymeropoulos, M. H.; Vos, H. L.; Ortiz de Luna, R. I.; Francomano, C. A. A nonsense mutation in the cathepsin K gene observed in a family with pycnodysostosis. *Genome Res.* **1996**, *6*, 1050–1055. (c) Gelb, B. D.; Shi, G.-P.; Chapman, H. A.; Desnick, R. J. Pycnodysostosis, a lysosomal disease caused by cathepsin K deficiency. *Science* **1996**, *273*, 1236–1238.
- (5) (a) Marquis, R. W. Inhibition of cysteine proteases. *Annu. Rep. Med. Chem.* **2000**, *35*, 309–320. (b) Veber, D. F.; Thompson, S. K. The therapeutic potential of advances in cysteine protease inhibitor design. *Curr. Opin. Drug Discovery Des.* **2000**, *3*, 362–369. (c) Yamashita, D. S.; Dodds, R. A. Cathepsin K and the design of inhibitors of cathepsin K. *Curr. Pharm. Des.* **2000**, *6*, 1–24. (d) Leung, D.; Abbenante, G.; Fairle, D. P. Protease inhibitors: current status and future prospects. *J. Med. Chem.* **2000**, *43*, 305–341. (e) Otto, H. H.; Schirmeister, T. Cysteine proteases and their inhibitors. *Chem. Rev.* **1997**, *97*, 133–171.
- (6) (a) Yamashita, D. S.; Smith, W. W.; Zhao, B.; Janson, C. A.; Tomaszek, T. A.; Bossard, M. A.; Levy, M. A.; Oh, H.-J.; Carr, T. J.; Thompson, S. T.; Ijames, C.; Carr, S. A.; McQueney, M.; D'Alessio, K. J.; Amegadzie, B. Y.; Hanning, C. R.; Abdel-Meguid, S.; DesJarlais, R. L.; Gleason, J. G.; Veber, D. F. Structure and design of potent and selective cathepsin K inhibitors. *J. Am. Chem. Soc.* **1997**, *119*, 11351–11352. (b) DesJarlais, R. L.; Yamashita, D. S.; Oh, H.-J.; Uzinskas, I. N.; Erhard, K. F.; Allen, A. C.; Haltiwanger, R. C.; Zhao, B.; Smith,

- W. W.; Abdel-Meguid, S. S.; D'Alessio, K.; Janson, C. A.; McQueney, M. S.; Tomaszek, T. A.; Levy, M. A.; Veber, D. F. Use of X-ray co-crystal structures and molecular modeling to design potent and selective non-peptide inhibitors of cathepsin K. *J. Am. Chem. Soc.* **1998**, *35*, 9114–9115. (c) LaLonde, J. M.; Zhao, B.; Smith, W. W.; Janson, C. A.; DesJarlais, R. L.; Tomaszek, T. A.; Carr, T. J.; Thompson, S. K.; Oh, H.-J.; Yamashita, D. S.; Veber, D. F.; Abdel-Meguid, S. S. Use of papain as a model for the structure-based design of cathepsin K inhibitors: Crystal structures of two papain-inhibitor complexes demonstrate binding to S'-subsites. *J. Med. Chem.* **1998**, *41*, 4567–4576.
- (7) Veber, D. F.; Yamashita, D. S.; Oh, H.-J.; Smith, B. R.; Salyers, K.; Levy, M.; Lee, C.-P.; Marzulli, A.; Smith, P. L.; Tomaszek, T.; Tew, D.; McQueney, M.; Stroup, G. B.; Lark, M. W.; James, I. E.; Gowen, M. Novel inhibitors of the osteoclast specific cysteine protease, cathepsin K. *Pept. New Millennium, Proc. Am. Pept. Symp., 16th* **2000**, 453–455.
- (8) Marquis, R. W.; Yamashita, D. S.; Ru, Y.; LoCastro, S. M.; Oh, H.-J.; Erhard, K. F.; DesJarlais, R. L.; Head, M. S.; Smith, W. W.; Zhao, B.; Janson, C. A.; Abdel-Meguid, S. S.; Tomaszek, T. A.; Levy, M. A.; Veber, D. F. Conformationally constrained 1,3-diaminoketones: a series of potent and selective inhibitors of the cysteine protease cathepsin K. *J. Med. Chem.* **1998**, *41*, 3563–3567.
- (9) Marquis, R. W.; Ru, Y.; Zeng, J.; Trout, R. E. L.; LoCastro, S. M.; Gribble, A. D.; Witherington, J.; Fenwick, A. E.; Garnier, B.; Tomaszek, T. A.; Tew, D.; Hemling, M. E.; Quinn, C. J.; Smith, W. W.; Janson, C. A.; Zhao, B.; McQueney, M. S.; D'Alessio, K. J.; Veber, D. F. Cyclic ketone inhibitors of the cysteine protease cathepsin K. *J. Med. Chem.* **2001**, *44*, 725–736.
- (10) Marquis, R. W.; Ru, Y.; Erhard, K. F.; Gribble, A. D.; Witherington, J.; Fenwick, A.; Garnier, B.; Bradbeer, J.; Lark, M.; Gowen, M.; Tomaszek, T. A.; Tew, D. G.; Zhao, B.; Smith, W. W.; Janson, C. A.; D'Alessio, K. J.; McQueney, M. S.; Abdel-Meguid, S. S.; Salyers, K. L.; Smith, B. R.; Levy, M. A.; Veber, D. F. Orally bioavailable inhibitors of the cysteine protease cathepsin K. 218th ACS National Meeting, New Orleans, LA, Aug 22–26, 1999; MEDI-019.
- (11) As examples:

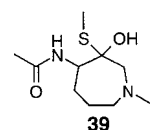


Cathepsin K $K_{i,app} > 1\mu\text{M}$ R = H; Cathepsin K $K_{i,app} = 0.18\text{ nM}$
 R = CH₃; Cathepsin K $K_{i,app} = 50\text{ nM}$

- (12) De Amici, M.; De Micheli, C.; Misani, V. Nitrile oxides in medicinal chemistry-2. Synthesis of the two diastereomers of dihydromuscimol. *Tetrahedron* **1990**, *46*, 1975–1986.
- (13) (a) Nguyen, S. T.; Johnson, L. K.; Grubbs, R. H.; Ziller, J. W. Ring-opening metathesis polymerization (ROMP) of polystyrene by group VIII carbene complex in protic media. *J. Am. Chem. Soc.* **1992**, *114*, 3974–3975. (b) Fu, G. C.; Grubbs, R. H. The application of catalytic ring-closing olefin metathesis to the synthesis of unsaturated oxing heterocycles. *J. Am. Chem. Soc.* **1992**, *114*, 5426–5427. (c) Miller, S. J.; Kim, S.-H.; Chen, Z.-R.; Grubbs, R. H. Catalytic ring-closing metathesis of dienes: application to the synthesis of eight-membered rings. *J. Am. Chem. Soc.* **1995**, *117*, 2108–2109. (d) Miller, S. J.; Grubbs, R. H. Synthesis of conformationally restricted amino acids and peptides employing olefin metathesis. *J. Am. Chem. Soc.* **1995**, *117*, 5855–5856. (e) Grubbs, R. H.; Chang, S. Recent advances in olefin metathesis and its application in organic synthesis. *Tetrahedron* **1998**, *54*, 4413–4450.
- (14) For a discussion of the factors influencing the nucleophilic ring opening of the 8-oxa-3-azabicyclo[5.1.0]octane ring system, see: (a) Tanner, D.; Almaro, A.; Högberg, T. Total synthesis of balanol, part 1. Enantioselective synthesis of the hexahydroazepine ring via chiral epoxides and aziridines. *Tetrahedron* **1995**, *51*, 6061–6070. (b) Tanner, D.; Tedenborg, L.; Almaro, A.; Petterson, I.; Csöregi, I.; Kelly, N. M.; Anderson, P. G.; Högberg, T. Total synthesis of balanol 2. Completion of the synthesis and investigation of the structure and reactivity of two key heterocyclic intermediates. *Tetrahedron* **1997**, *53*, 4857–4868.
- (15) Bayley, H.; Standing, D. N.; Knowles, J. R. Propane-1,3-dithiol: a selective reagent for the efficient reduction of alkyl and aryl azides to amines. *Tetrahedron Lett.* **1978**, *39*, 3633–3634.
- (16) Parikh, J. R.; Doering, v. W. E.; Sulfur trioxide in the oxidation of alcohols by dimethyl sulfoxide. *J. Am. Chem. Soc.* **1967**, *89*, 5505.
- (17) (a) Yamashita, D. S.; Dong, X.; Oh, H.-J.; Brook, C. S.; Tomaszek, T. A.; Szewczuk, L.; Tew, D. G.; Veber, D. F. Solid-phase synthesis of a combinatorial array of 1,3-bis(acylamino)-2-butanones, inhibitors of the cysteine proteases cathepsins K and L. *J. Comb. Chem.* **1999**, *1*, 207–215.
- (18) Greenlee, W. J.; Springer, J. P.; Patchett, A. A. Synthesis of an analogue of tabtoxinine as a potential inhibitor of D-alanine: D-ligase (ADP forming). *J. Med. Chem.* **1989**, *32*, 165–170.
- (19) Albeck, A.; Persky, R. Stereocontrolled synthesis of erythro N-protected α -amino epoxides and peptidyl epoxides. *Tetrahedron* **1994**, *50*, 6333–6346.
- (20) (a) Liskamp, R. M. J. Conformationally restricted amino acids and dipeptides, (non)peptidomimetics and secondary structure mimetics. *Recl. Trav. Chim. Pays-Bas*, **1994**, *113*, 1–19. (b) Marshall, G. R.; Fedric, G. A.; Moore, M. L. Peptide conformation and biological activity. *Annu. Rep. Med. Chem.* **1978**, *13*, 227.
- (21) James, I. E.; Lark, M. W.; Zembryki, D.; Lee-Ryckwzski, E. V.; Hwang, S. M.; Tomaszek, T. A.; Belfiore, P.; Gowen, M. Development and characterization of a human *in vitro* resorption assay: demonstration of utility using novel antiresorptive agents. *J. Bone Miner. Res.* **1999**, *14*, 1562–1569.
- (22) Dodds, R. A.; James, I. E.; Rieman, D.; Hwang, S.-M.; Ahern, R.; Connor, J. R.; Thompson, S.; Veber, D.; Drake, F. H.; Holmes, S.; Lark, M. W.; Gowen, M. Human osteoclast cathepsin K is processed intracellularly prior to attachment and bone resorption. *J. Bone Miner. Res.* **2001**, *16*, 478–486.
- (23) The synthesis of deuterated analogues **37** and **38** is shown below:



- (24) McQueney, M. S.; Feild, J.; Hanning, C. R.; Brun, K.; Ramachandran, K.; Connor, J.; Drake, F.; Jones, C. S.; Amegadzie, B. Y. Cynomolgus monkey (*Macaca fascicularis*) cathepsin K: cloning, expression, purification and activation. *Protein Express. Purif.* **1998**, *14*, 7–394.
- (25) Feild, J.; Brun, K.; Hanning, C. R.; Tomaszek, T.; Amegadzie, B.; D'Alessio, K. J.; Yamashita, D. S.; Oh, H.-J.; Veber, D. F.; Lark, M. W.; McQueney, M. Characterization of rat cathepsin K. Submitted for publication.
- (26) Stroup, G. B.; Lark, M.; Veber, D. F.; Bhattacharyya, A.; Blake, S.; Dare, L. C.; Erhard, K. F.; Hoffman, S. J.; James, I. E.; Marquis, R. W.; Ru, Y.; Vasko-Moser, J. A.; Smith, B. R.; Tomaszek, T.; Gowen, M. Potent and selective inhibition of cathepsin K leads to inhibition of bone resorption *in vivo* in a nonhuman primate. Submitted for publication.
- (27) Lark, M. W.; Stroup, G. B.; James, I. A.; Dodds, R. A.; Hwang, S.-M.; Blake, S. M.; Lechowska, B. A.; Hoffman, S. J.; Smith, B. R.; Kapadia, R.; Erhard, K.; Ru, Y.; Dong, X.; Marquis, R. W.; Veber, D.; Gowen, M. Inhibition of cathepsin K with the small molecule, nonpeptidic inhibitor SB-331750, prevents bone matrix resorption in the ovariectomized rat. Submitted for publication.
- (28) Ring conformation and relative positions of the proximal pendant groups were analyzed by modeling both diastereomers of the representative thiohemiketal **39**:



- (29) Hunter, C. A.; Sanders, J. K. M. The nature of π - π interactions. *J. Am. Chem. Soc.* **1990**, *112*, 5525–5534.
- (30) (a) Smith, A. B., III; Guzman, M. C.; Sprengler, P. A.; Keenan, T. P.; Holcomb, R. C.; Wood, J. L.; Carroll, P. J.; Hirschmann, R. *De novo* design, synthesis and X-ray crystal structures of the pyrrolidinone-based β -strand peptidomimetics. *J. Am. Chem. Soc.* **1994**, *116*, 9947–9962; see also refs 9 and 10 of this article. (b) Smith, A. B., III; Keenan, T. P.; Holcomb, R. C.; Sprengler, P. A.; Guzman, M. C.; Wood, J. L.; Carroll, P. J.; Hirschman, R. *J. Am. Chem. Soc.* **1992**, *114*, 10672–10674. (c) Fairlie, D. P.; Tyndall, J. D. A.; Reid, R. C.; Wong, A. K.; Abbenante, G.; Scanlon, M. J.; March, D. R.; Bergman, D. A.; Chai, C. L. L.; Burkett, B. A. *J. Med. Chem.* **2000**, *43*, 1271–1281.

- (31) Lipinski, C. A.; Lombardo, F.; Dominy, B. W.; Feeney, P. J. Experimental and computational approaches to estimate solubility and permeability in drug discovery. *Adv. Drug Deliv. Rev.* **1997**, *23*, 3–25.
- (32) Navia, M. A.; Chattervedi, P. R. Design principles for orally bioavailable drugs. *Drug Discovery Today* **1996**, *1*, 179–189.
- (33) Chan, O. H.; Stewart, B. H. Physicochemical and drug-delivery considerations for oral bioavailability. *Drug Discovery Today* **1996**, *1*, 461–473.
- (34) (a) Benet, L. Z.; Wu, C.-Y.; Hebert, M. F.; Wachter, V. J. Intestinal drug metabolism and antitransport processes: A potential paradigm shift in oral drug delivery. *J. Controlled Release* **1996**, *39*, 139–143. (b) Wachter, V. J.; Silverman, J. A.; Zhang, Y.; Benet, L. Z. Role of P-glycoprotein and cytochrome P-450 3A in limiting oral absorption of peptides and peptidomimetics. *J. Pharm. Sci.* **1998**, *87*, 1322–1330.
- (35) Smith, P. L. Methods for evaluating intestinal permeability and metabolism *in vitro*. In *Methods for assessing drug absorption and metabolism*; Borchardt, R. T., Smith, P. L., Wilson, G., Eds.; Plenum Press: New York, 1996; pp 13–3.
- (36) Ariens, E. J. Stereochemistry, a basis for sophisticated nonsense in pharmacokinetics and clinical pharmacology. *Eur. J. Pharmacol.* **1984**, *26*, 663–668.
- (37) (a) Spatola, A. Peptide backbone modifications: structure–activity analysis of peptides containing amide bond surrogates, conformational constraints and related backbone replacements. *Chem. Biochem. Amino Acid Pept. Proteins* **1983**, *7*, 267–357. (b) Conradi, R. A.; Hilgers, A. R.; Ho, N. F.; Burton, P. S. The influence of peptide structure on transport across caco-2 cells. II. Peptide bond modification which results in improved permeability. *Pharm. Res.* **1992**, *9*, 435.
- (38) Wachter, V. J.; Wu, C.-Y.; Benet, L. Z. Overlapping substrate specificities and tissue distribution of cytochrome P450 3A and P-glycoprotein: Implications for drug delivery and activity in cancer chemotherapy. *Mol. Carcinogen.* **1995**, *3*, 129–134.
- (39) (a) Gottesman, M. M.; Pastan, I.; Ambudkar, S. V. P-glycoprotein and multidrug resistance. *Curr. Opin. Genet. Dev.* **1996**, *6*, 610–617. (b) Gottesman, M. M.; Pastan, I. Biochemistry of multidrug resistance mediated by the multidrug transporter. *Annu. Rev. Biochem.* **1993**, *62*, 385–427.
- (40) Zhao, B.; Janson, C. A.; Amegadzie, B. Y.; D'Alessio, K.; Griffin, C.; Hanning, C. R.; Jones, C.; Kurdyla, J.; McQueney, M.; Qiu, X.; Smith, W. W.; Abdel Meguid, S. S. Crystal structure of human osteoclast cathepsin K complex with E-64. *Nat. Struct. Biol.* **1997**, *4*, 109–111.
- (41) Mohamadi, F.; Richards, N. G. J.; Guida, W. C.; Liskamp, R.; Lipton, M.; Caufield, C.; Chang, G.; Hendrickson, T.; Still, W. C. MacroModel – an integrated software system for modeling organic and bioorganic molecules using molecular mechanics. *J. Comput. Chem.* **1990**, *11*, 440–467.
- (42) (a) Halgren, T. A. Merck molecular force field. I. Basis, form, scope, parametrization, and performance of MMFF94. *J. Comput. Chem.* **1996**, *17*, 490–519. (b) Halgren, T. A. MMFF VI. MMFF94's option for energy minimization studies. *J. Comput. Chem.* **1999**, *20*, 720–729.
- (43) Still, W. C.; Tempczyk, A.; Hawley, R. C.; Hendrickson, T. Semianalytical treatment of solvation for molecular mechanics and dynamics. *J. Am. Chem. Soc.* **1990**, *112*, 6127.
- (44) Gabrielsson, J.; Weiner, D. *Pharmacokinetic and Pharmacodynamic Data Analysis*; Apotekarsocieteten: Stockholm, 1997.

JM000481X